Fascin1 accelerates serrated pathway carcinogenesis by remodeling adherens junctions and restoring Wnt signaling.

Short title: Fascin1 accelerates serrated pathway colon cancers.

Amin Esmaeilniakooshkghazi[1*], Eric Pham[1*], Sudeep P. George[1], Afzal Ahrorov[1], Fabian R. Villagomez[1], Michael Byington[4], Srijita Mukhopadhyay[2], Srinivas Patnaik[1,3], Jacinta C. Conrad[4], Monali Naik[1], Saathvika Ravi[1], Niall Tebbuttt[5], Jennifer Mooi[5], Camilla M Reehorst[5], John M. Mariadason[5], Seema Khurana[1,6@]

[1] Department of Biology and Biochemistry, University of Houston, Houston TX 77204

[2] Department of Biology and Biochemistry, Center for Nuclear Receptors and Cell Signaling, University of Houston, Houston 77204, TX

[3] Current address: School of Biotechnology Campus XI, KIIT University, Bhubaneswar, Odisha 751024, India

[4] Department of Chemical and Bimolecular Engineering, University of Houston, Houston TX 77204

[5] Gastrointestinal Cancers Programs, Olivia Newton-John Cancer Research Institute, and La Trobe University School of Cancer Medicine, Melbourne, Victoria, Australia

[6] School of Allied Health Sciences, Baylor College of Medicine, Houston TX 77030

*** Both authors contributed equally to this manuscript.**

Grant Support: This study was supported by National Institutes of Diabetes and Digestive Kidney Diseases (grant DK-117476 to S.K.); and the Public Health Service (grant DK-56338).

Abbreviations: AJ, adherens junctions; CRC, colorectal carcinoma; E/M, hybrid epithelial-mesenchymal; GI, gastrointestinal; nAJ, nascent adherens junctions; SSL, sessile serrated lesions; TJ, tight junction; TM, tumor microtube; TNT, tunneling nanotube.

Correspondence and requests for materials should be addressed to: Seema Khurana, Ph.D., Department of Biology and Biochemistry, 369 Science and Research Building SR2, Room 421E, 3455 Cullen Blvd., Houston, Texas 77004. E-mail: skhurana@central.uh.edu; Tel: 713-743-2705.

***Disclosures*:** The authors declare no potential conflict of interest exists.

Preprint server: bioRxiv.org

Word Count: 5785

Author Contributions: Eric Pham, Amin Esmaeilniakooshkghazi, Sudeep P. George, Afzal Ahrorov, Fabian R. Villagomez, Michael Byington, Srijita Mukhopadhyay, Srinivas Patnaik, Monali Naik and Saathvika Ravi, Niall Tebuttt, Jennifer Mooi, Camilla M. Reehorst performed the experiments described in this study. Jacinta C. Conrad analyzed the migration data and provided important guidance for the experimental design of these studies. John M. Mariadason is a long-standing collaborator of the contributing author and provided the patient cohort data, analyzed the patient cohort data as well as provided valuable suggestions during the writing of this manuscript.

Data Transparency: Data, analytical methods, and study material will be made available to other researchers once the study has been completed and published.

Synopsis: Our study demonstrates the key role fascin1 plays in serrated pathway colorectal cancers by generating a cooperating signaling pathway that reverses BRAF^{V600E}-induced senescence and differentiation to accelerate tumor growth and metastasis. We show that by remodeling adherens junction mechanotransduction fascin1 activates oncogenic Wnt signaling which renders colon epithelial cells responsive to mutational activation of BRAF^{V600E}. Our findings could impact the development of novel therapies for serrated pathway CRCs that target fascin1 and/or Wnt pathway genes.

Abstract

Approximately 35% of colorectal carcinomas (CRCs) arise from sessile serrated lesions (SSLs) which have a >90% rate of BRAF^{V600E} mutation. Compared to conventional CRCs, serrated pathway CRCs (SCRCs) are more aggressive, lack treatment options, and have a poorer outcome. Paradoxically, the oncogene BRAF^{V600E} induces differentiation and senescence and requires additional factors that reduce differentiation *via* Wnt-dependent mechanism, to initiate and sustain serrated pathway tumorigenesis. The mechanism modulating Wnt activation in BRAF^{V600E}-driven colon cancers remains unresolved. The actin-bundling protein fascin1 is expressed throughout the developing gut but its expression is lost in the adult gastrointestinal tissue. Fascin1 is re-expressed in SSLs and in SCRCs, where its upregulation is linked to aggressive disease, poor prognosis and increased mortality. Nonetheless, the role of fascin1 in the etiology of SCRCs remains unidentified. Here we show, for the first time, that in BRAF^{V600E}-driven SCRCs, fascin1 remodels adherens junction mechanotransduction to activate oncogenic Wnt signaling which accelerates and amplifies tumor growth and metastasis. In this study we describe the key role fascin1 plays by generating a cooperating signaling pathway that facilitates the initiation and progression of BRAF^{V600E}-driven SCRCs. Our findings could impact the development of novel therapies for SCRCs that target fascin1 and/or Wnt pathway genes.

Background & Aims

While the adenoma-carcinoma pathway is the major contributor to sporadic CRCs, evidence accumulated over the last decade shows that approximately 35% of CRCs arise *via* the alternative serrated pathway.[1] Compared to conventional CRCs, the serrated pathway CRCs (SCRCs) are less well understood and carry a worse prognosis.[1] These tumors arise from malignant sessile serrated lesions (SSLs; hitherto called sessile serrated adenomas/polyps) and >90% of these lesions contain an activating *BRAF*^{V600E} mutation which amplifies MAPK signaling.[1, 2] While ~35% of CRCs arise from precursor lesions with serrated glands, <10% of CRCs manifest a serrated morphology at diagnosis. *BRAF*^{V600E} mutation occurs early, is associated with advanced CRC and defines a sub-population associated with a more aggressive disease course, reduced progression-free and overall survival, and treatment resistance.[2, 3] While selective inhibitors of *BRAF*^{V600E} have been successfully used to treat metastatic melanomas these agents have minimal benefit as single agents in refractory *BRAF*^{V600E} metastatic CRCs and BRAF mutation is considered a negative predictive marker of epidermal growth factor receptor (EGFR) antibody treatment response.[4, 5] The clinical benefit of adding EGFR antibody treatment in BRAF^{V600E}-driven SCRCs is also minimal and remains controversial underscoring the critical need to find new treatment with better clinical outcomes for these patients.[6-8]

Compared to conventional CRCs, the biological underpinnings of BRAF-mutant CRC are complex and remain poorly understood. Nevertheless, abnormal Wnt activation is a prominent feature of SSLs that occurs in the absence of mutations in the APC/β-catenin pathway and early changes in Wnt signaling are required for the dysplastic and

neoplastic progression of intestinal lesions with BRAF^{V600E} mutation.[9, 10] Wnt activation in SCRCs has also been linked to early neoplastic progression and poor prognosis.[9, 11] Moreover, resistance to targeted therapy BRAF^{V600E} inhibitors is a major challenge that is also linked to activation of Wnt pathway genes.[12, 13] Paradoxically, ectopic expression of oncogenic BRAF^{V600E} promotes senescence or differentiation of intestinal stem cells consequently BRAF^{V600E} mutation by itself is deemed inefficient in triggering or sustaining serrated pathway tumorigenesis.[11, 14, 15] Consequently, while oncogenic BRAF^{V600E} mutation eventually leads to tumors in mouse models, tumor growth is very slow.[16, 17] This is not unique to the intestine and expression of BRAF^{V600E} in other mouse models of human cancers also induces senescence-like proliferative arrest.[18] Oncogene-induced senescence is a conserved defense mechanism that limits the development of cancer by arresting the proliferation of damaged or stressed cells such as stem cells or other cancer initiating cells that are at risk for malignant transformation[19].[20] Loss of intestinal differentiation-promoting transcription factors that are antagonistic to Wnt signaling restores the tumorigenic capability of BRAF^{V600E} and accelerates colon tumor growth in mice, emphasizing the need for sustained Wnt activation for oncogenic BRAF^{V600E} to initiate and advance serrated pathway tumorigenesis.[11] Nonetheless, the molecular mechanism that regulates oncogenic Wnt activation in SSLs and BRAF^{V600E}-driven SCRCs remains unresolved. Similarly, while the underlying genes that drive serrated pathway carcinogenesis remain unidentified, the BRAF^{V600E} mutation has been linked to profound cellular changes specifically tumor dedifferentiation, cytoskeletal reorganization and remodeling of adherens junctions (AJs) and tight junctions (TJs).[21-24] How these changes influence serrated pathway tumorigenesis or the molecular mechanism

responsible for these cellular changes also remains unidentified. Ascertaining and understanding the role of these novel genes is, however, crucial in designing management approaches and therapies for these pharmacologically intractable CRCs.

Fascin1 is an actin-bundling protein that is expressed throughout the gastrointestinal (GI) tissue in the mucosa and the muscle layers during mouse and human development.[25, 26] Notably, fascin1 expression in the developing GI tissue is intense in regions of ongoing differentiation, cell migration, and cell proliferation indicative of a role for fascin1 in cell-cell interactions, cell division, and cell growth during GI development.[25, 26] Nevertheless, fascin1 transcript and protein are absent from normal adult intestinal epithelium.[26] However fascin1 is re-expressed in CRCs, where its expression has been correlated with a clinically aggressive disease with a higher incidence of metastasis and poor prognosis.[27-30] In multivariate analysis, fascin1 has been identified as an independent factor for CRCs, and fascin1 positive CRCs exhibit a greater ability to invade lymph nodes and develop extra-nodal tumor extensions, and have a higher likelihood of recurrence with a lower rate of disease-free and overall survival.[27, 31, 32] Even though fascin1 has been associated with aggressive clinical features of CRCs, the exact mechanism that mediates fascin1-dependent colon tumor growth and metastasis remains unclear. It is assumed that fascin1 drives tumor cell migration and invasion by assembling filopodia and invadopodia. However, there is emerging evidence that fascin1 also has cell migration-independent functions linked to tumor cell proliferation, oncogenesis, metastatic colonization, anoikis resistance, chemoresistance, and cancer stemness although the molecular mechanism underlying these non-canonical functions of fascin1 remain unclear.[31, 33, 34] Consequently, the mechanism by which fascin1 fosters metastatic

CRCs remains unknown. Multiple studies have now identified fascin1 as a marker of SSLs and fascin1 is significantly (~12 fold) and specifically upregulated in SSLs but not conventional colorectal polyps.[2, 35-37] An expression profile of CRCs has identified fascin1 expression specifically in SCRCs but not conventional CRCs identifying fascin1 also as a marker of SCRCs.[21] Moreover, in SCRCs fascin1 expression has been correlated with both BRAF and KRAS mutations.[21] Despite that the function of fascin1 in the etiology of SCRCs has not been directly investigated. The functional characterization of fascin1 in SSLs and SCRCs could shed light on the biology driving serrated pathway cancers.

Using a large cohort of CRC patients, we show that fascin1 is upregulated in one-third of all CRCs, which correlates with fascin1 upregulation in all SCRCs. This underscores the need to better understand the role of fascin1 in colorectal carcinogenesis. Our study also shows that fascin1 expression correlates with more poorly differentiated/high grade CRCs, which grow and metastasize more rapidly. Our results demonstrate that fascin1's canonical cell migration-dependent and its non-canonical function linked to tumor cell proliferation and de-differentiation both contribute to BRAF^{V600E}-driven tumorigenesis. In this study, we show for the first time, that fascin1 remodels AJ mechanotransduction to activate oncogenic Wnt signaling which accelerates BRAF^{V600E}-driven colorectal tumor growth and metastasis. Our study identifies fascin1's direct role in oncogenic mechanisms that drive serrated pathway CRCs which could play an important role in both the response of BRAF-mutated CRC cells to targeted therapies but could also lead to the development of novel therapies for the treatment of BRAF^{V600E}-driven CRCs.

Methods

Cells and plasmids: HT-29/19A, HCT-116 and MDCK cells are described by us previously.[88, 89] MRC-5, HT-29 cells were purchased from American Type Culture Collection (ATCC, Rockville, MD). Human fascin1 plasmid was a kind gift from Dr. Shigeko Yamashiro (Rutgers University, New Brunswick, NJ). HT-29/19A and HCT-116 cells were transduced with lentivirus expressing short-hairpin RNAs (shRNAs) targeting fascin1 (Sigma-Aldrich, St. Louis, MO). For the rescue experiments, EGFP-Fascin1 plasmid without 3'UTR region were overexpressed in HT-29/19A-shF cells. EGFP-Fascin1 or EGFP were also overexpressed in HT-29 cells that lack endogenous fascin1 protein.

Tumor spheroid culture: Tumor spheroids were generated as described previously.[90] Briefly, cells were grown on standard tissue culture dishes to 80% confluence, and re-plated 24 h prior to initiating tumor spheroids. For tumor spheroids 1 x10^6 cells/mL were plated on agarose-coated dishes. Spheroids were imaged using a Nikon Eclipse TE2000-U inverted microscope equipped with a CoolSnap ES charge-coupled device (CCD) camera. For hanging drop cultures, 2000 cells in 20 µl drops were plated on the inside lids of 10 cm dishes, and the lids were inverted prior to incubation.

Immunoblotting: Cell lysates were prepared as described previously.[91] Briefly, proteins were separated by SDS-PAGE, transferred to nitrocellulose membranes, immunoblotted and detected with ECL. All Western blots are representative of at least three independent experiments with similar findings.

Cell migration assay: Migration assay was performed as described previously.[65] Briefly, cells were plated on 6-well tissue culture treated dishes and allowed to grow to confluence. Upon confluence, the monolayers were wounded with a sterile blade. Wells were rinsed with phosphate buffered solution (PBS), and cells were treated with MRC-5 conditioned media (diluted in 3 volumes 10% FBS DMEM). Cells were treated for 20 h prior to imaging.

Scratch-wound image analysis: For image analysis, cells were identified through a series of filters applied to individual images using Python, which produced binary images. Adjacent frames were shifted to maximize the total overlap in the binary images and cells were assigned to tracks based on maximum overlap. Cells unaccounted for by this method were assigned tracks by minimizing the centroid displacement between remaining cells. Edge cells were identified as being within 75 μm of the migratory front. Loose and bulk cells were identified by their position relative to the migratory front and edge cells. Instantaneous centroid velocities were used for further analysis. Cell tracks that were detected in a minimum of 10 frames were analyzed.

Cell-cell junction remodeling assay: For mature AJ remodeling assays, $5x10^4$ cells were plated in 6-well tissue culture treated dishes and allowed to form small colonies (<40 cells). The cells were treated with MRC-5 conditioned media, and imaged every 5 minutes. Images were taken with a Nikon Eclipse TE2000-U inverted microscope and CoolSnap ES CCD camera.

Invasion Assay: For invasion assays, tumor spheroids formed by the hanging drop method were isolated 96 hours after suspension culture, and embedded in a Collagen I matrix (2mg/mL). The Collagen I matrix was allowed to solidify for 90 minutes prior to being overlaid with 10% FBS containing DMEM with 50 ng/mL HGF. Additionally, the tumor spheroids were treated with vehicle control (DMSO). The invasion occurred over 8 days.

Soft agar colony formation assay: First a layer of 0.5% agarose-containing DMEM was solidified at the bottom of wells of 6-well dishes to prevent cells from attaching. Cells were mixed into liquid 0.33% agarose at the desired cell numbers and allowed to solidify on top of the 0.5% layer. For HT-29/19A cells 500 cells were used. Colonies greater than 0.05μm^2 in area were counted.

Mice: NOD-*scid* IL2Rgamma^{null} mice (NSG) (Jackson Laboratory, Bar Harbor, ME) were injected subcutaneously with 2 x 10^6 Scr and shF cells and intra-splenic with 1x10^6 Scr and shF cells. Three weeks' post-injection primary and secondary tumors were excised and measured.

Zebrafish metastasis assay: Zebrafish (Danio rerio) were reared and maintained at 28.5^{o}C. *Tg(kdrl:EGFP)mitfa$^{b692/b692}$* was generated by crossing *Tg(kdrl:EGFP)* with *mitfa$^{b692/b692}$* (Zebrafish International Resource Center, Eugene, OR). 300-500 HT-29/19A Scr and HT-29/19A-shF cells labeled with CM-Dil (ThermoFisher) were microinjected into yolk sac of 2-day old embryos using a pressure injector (Harvard Apparatus, Holliston,

MA) and manipulator (MM33-Righ, Märzhäuser Wetzlar, Germany). Embryos and cells injected in the yolk were incubated at 34ºC and imaged using OLYMPUS IX51 fluorescence microscope, OLYMPUS XM10 camera and cellSens Dimension software (Olympus, Center Valley, PA, USA).

Immunofluorescence and live cell fluorescence microscopy: Confocal images were acquired using the Olympus FV2000 inverted confocal microscope. Unless otherwise indicated all data were obtained by performing three independent experiments with n = 10 fields/group and >300 cells/group were analyzed each time. Nuclei were counter stained with DAPI. Tumor spheroids were studied in three independent experiments with 10 spheroids per group in each experiment. Plot profiles were generated by measuring the distribution of AJ associated proteins in regions of interest (ROI) highlighted by a white line, 10 μm long.

Chromatin Immunoprecipitation. ChIP was carried out as previously described.[92] Briefly, cells were fixed with 1.5% paraformaldehyde, lysed, nuclei were purified, and then chromatin was sheared by sonification. Immunoprecipitation was carried out with β-catenin monoclonal antibody and Protein G magnetic beads (Sigma-Aldrich). For PCR, the following primers were used:

MMP9:

F: 5’-CCTCCTTAAAGCCCCCACAA-3’,

R: 5’-CAGTCCACCCTTGTGCTCTT-3’;

CCND1:

F: 5’-CAGAAGAGCGCGAGGGAG-3’,

R: 5’-ATGGAACACCAGCTCCTGTG;

MYC,

F: 5’-GAGGCGAACACACAACGTCTT-3’,

R: 5’-CGCAACAAGTCCTCTTCAGAAA-3’

MMP9 negative control,

F: 5’-GTGGGACCTCAACGTCTGTC-3’,

R: 5’- CACCACCTCTAAGCACTGACAT-3’.

Fascin1:

F: 5’-AGGCGGCCAACGAGAGGAAC-3’

R: 5’-ACGATGATGGGGCGGTTGAT’3’

CD44:

F: 5’-GCAGTCAACAGTCGAAGAAGG’3’

R: 5’-TGTCCTCCACAGCTCCATT-3’

MMP7:

F: 5’-CTTACCTCGGATCGTAGTGG-3’

R: 5’-CCCCAACTAACCCTCTTGAAGT-3’

AXIN2:

F: 5’-AACCTATGCCCGTTTCCTCTA-3’

R: 5’-GAGTGTAAAGACTTGGTCCACC-3’

TCF1:

F: 5’-CCAGTGTGCACCCTTCCTAT-3’

R: 5’-AGCCCCACAGAGAAACTGAA-3’

Promoter reporter assays. Promoter reporter assays. Cells were transfected in 24-well dishes using Lipofectamine 2000 (ThermoFisher) with β-catenin reporter Super 8X TOPFlash and pSV-β-Galactosidase control vector. All cells were lysed approximately 24 hours post-transfection, and luciferase activity was measured with Luciferase Assay (Promega, Madison, Wisconsin, USA) and β-Galactosidase with chlorophenol red-β-D-galactopyranoside (CPRG). Reporter activity was normalized to β-Galactosidase activity. 24 hours’ post-transfection, cells were treated with DMSO, 20µM G2, or 100µM G2 for 24 hours. Luminescence was quantified with VICTOR Multilabel Plate Reader (PerkinElmer, Waltham, MA, USA).

Fascin1 and β-catenin immunohistochemistry scoring: Patient tumor microarrays were immunostained for fascin1 and total β-catenin. Fascin1 was scored using the method of Hashimoto *et al* and β-catenin was scored by adapting the method of Hugh *et al*.[27, 93] Immunohistology in paired tumor panels show expression of fascin1 and β-catenin in the same tumor.

Statistical Analysis: Data are expressed as mean ± standard deviation (SD) or ± standard error (SE). Significance was determined by Student's t-test, Mann-Whitney U test, Kuiper's test, or Watson U2 test.

Study approval: All animal studies were performed in accordance with animal protocols approved by the University of Houston Institutional Animal Care and Use Committee.

All authors had access to the study data and have reviewed and approved the final manuscript.

Results

Fascin1 is upregulated in one-third of all CRCs and its expression correlates with poorly differentiated CRCs. Varying rates of fascin1 expression in CRCs have been reported. To characterize fascin1's role in SCRCs, we elected first to analyze fascin1 expression in a large cohort of 299 stage IV CRCs, from patients who participated in the Phase III MAX clinical trial.[38] Analysis of fascin1 expression using the Hashimoto *et al* scoring criteria revealed low to high fascin1 expression in 34.4% of cases (score 1-3) while 22.4% of cases expressed moderate to high fascin1 protein levels (score 2-3; Fig 1A).[27] These numbers parallel more closely the numbers estimated for SCRCs and suggest that fascin1 is likely expressed in all SCRCs. Additionally, in this patient cohort we found that fascin1 was more highly expressed in high grade/poorly differentiated CRCs (G1>G2>G3; Fig 1B) confirming fascin1's association with colorectal tumors with aggressive growth and metastatic potential.

In mutant BRAF^{V600E} CRC cells fascin1 remodels adherens junctions and forms ultra-long and large tumor microtube-like intercellular connections. To identify the functional role of fascin1 in the pathogenesis of tumors arising *via* the serrated/*BRAF^{V600E}* pathway, we performed loss-of-function studies by knockdown (KD) of fascin1 in *BRAF^{V600E}* mutant HT-29/19A CRC cells. Fascin1 targeting shRNAs markedly reduced endogenous fascin1 protein expression in the parental cell line but did not affect EGFP-Fascin1 overexpression confirming on-target specificity of the shRNA constructs (Supplementary Fig 1A).[22, 39, 40] Spheroids of HT-29/19A cells expressing scrambled shRNA (HT-29/19A-Scr) grew as loosely aggregated clusters of cells with a 'grape-like

morphology.' Comparatively, fascin1 KD cells (HT-29/19A-shF) formed tightly organized, compact spheres (Fig 1C), implicating a role for fascin1 in the remodeling of cell-cell adhesions. In sub-confluent cell cultures, HT-29/19A-Scr cells formed nascent cell-cell adhesions that appeared as long filopodia-like protrusions that morphed into lamellipodia-like structures at the distal ends as two cells established cell-cell contact (Fig 1D). In contrast, HT-29/19A-shF cells extended much smaller lamellipodial protrusions as two cells approached each other, similar to nascent adherens junction (nAJ) assembly by normal intestinal epithelial cells.[41] Notably, Scr cells formed these protrusions even in the absence of direct cell-cell contact highlighting fascin1's autonomous role in generating these large cell surface protrusions (Supplementary Fig 1B). Alternatively, Scr cells formed long intercellular conduits that lacked lamellipodia-like distal ends (Fig 1E). These remodeled cell-cell junctions contained fascin1, F-actin and tubulin (Figs 1D-1E) as well as E-cadherin indicating these protrusions are nAJs (Fig 1F). In these nAJs, fascin1 localized to both the filopodia-like and lamellipodia-like protrusions. By measuring the rate of assembly, we determined that fascin1, F-actin and tubulin are required to assemble these nAJs (Supplementary Figs 1C-1D). In normal intestinal epithelial cells, AJs are assembled by a symmetrical 'push and pull' mechanism.[42] Remarkably, fascin1 expressing Scr cells assembled AJs asymmetrically, where only one cell extended the protrusion (Cell 1, Fig 2A) with a lamellipodia-like distal end (red arrowhead) or long intercellular conduits (cyan arrowhead) while the neighboring cell assembled actin bundles that appear like stress fibers and attach to the E-cadherin and β-catenin foci (white arrowheads). In contrast, shF cells assembled AJs symmetrically where both cells generated similar protrusions and display similar actin organization overlapping with the

cortical actin. Gain-of-function studies performed by overexpression of EGFP tagged fascin1 in the non-transformed epithelial cells, MDCK (Supplementary Fig 1E) also resulted in the assembly of these ultra-long nAJs similar to HT-29/19A cells (Figs 2B). Notably, some MDCK EGFP-Fascin1 cells also initiated nAJ assembly by forming protrusions that resembled the sprouting phenotype of endothelial cells undergoing anastomosis (Fig 2C); or had a growth cone-like morphology (Fig 2D) reminiscent of fascin1's function in these tissue. More remarkably, these ultra-long nAJs are large enough to encompass functional mitochondria and lysosomes (Fig 2E).

These ultra-long AJs also formed in confluent cell cultures connecting two non-adjacent and significantly distant cells (Fig 3A, cell 1 is connected to cell 6). These remodeled AJs hovered over the confluent monolayer, which facilitated two distant cells to connect in this manner (Fig 3B). To analyze how fascin1 remodels 'mature' AJs, small clusters of MDCK EGFP and MDCK EGFP-Fascin1 cells were stimulated with hepatocyte growth factor (HGF) at concentrations that do not induce epithelial cell scatter. While the MDCK EGFP cells maintained cell-cell adhesions similar to normal epithelial cell clusters with few short-lived changes (Supplementary Video 1, Fig 3C), the MDCK EGFP-Fascin 1 cells continuously remodeled their cell-cell adhesions, dissolving and reforming them resulting in loosely connected cell clusters (Supplementary Video 2, Fig 3C). These dynamically remodeled cell-cell adhesions differed in length and lifespan which were positively correlated (Fig 3D). Morphologically similar structures called tunneling nanotubes (TNTs) are short-lived intercellular bridges with lifespans of less than 60 min while tumor microtubes (TMs) have lifespans greater than 60 min.[43, 44] Based on the

morphological characteristics of these intercellular junctions and their lifespan, we refer to these intercellular connections assembled by fascin1 as tumor microtube-like (TM-like).

Fascin1 transforms adherens junction mechanotransduction in BRAF^{V600E} CRC cells. In epithelial cells, the actin cytoskeleton is important for the stabilization of AJs, but it is also the force-generating mechanism required for AJ remodeling and it regulates AJ mechanotransduction.[45-47] In normal intestinal epithelial cells, mature AJs are stable, continuous, and associated with actin bundles running parallel to the plasma membrane overlapping with the cortical actin.[48] However, fascin1 expressing mutant *BRAF* HT-29/19A cells have AJs with actin bundles arranged perpendicular to the plasma membrane that appear as intercellular stress fibers forming end-on attachments with the discontinuous E-cadherin foci (Fig 4A, Top). Such discontinuous AJs have been seen in other cancer cells however, their role in tumorigenesis is unknown. [49, 50] In stark contrast, fascin1 KD cells formed continuous AJs with F-actin and E-cadherin distribution overlapping with the cell-cell margins similar to normal intestinal epithelial cells. There was no discernable difference in the lateral junctions between Scr and shF cells (Fig 4A, Middle). Gain-of-function studies performed by overexpressing EGFP-Fascin1 in the *BRAF^{V600E}* cell line HT-29 which lacks endogenous fascin1, confirmed fascin1's direct role in the remodeling of AJ associated actin cytoskeleton (Supplementary Figs 2A-2B). This function of fascin1 was also recapitulated in the non-transformed MDCK cells overexpressing EGFP-Fascin1 (Supplementary Fig 2C); and in the rescue experiments performed in the fascin1 KD shF cells by overexpressing EGFP-Fascin1 (Supplementary

Fig 2D). Together, these data demonstrate that fascin1's function in AJ remodeling is not cell type-specific and is independent of oncogenic transformation.

In vitro fascin1 and α-actinin mutually exclude each other to form discrete fascin1 or α-actinin cross-linked actin networks.[51] We reasoned that in *BRAF*^{V600E} CRC cells, fascin1 expression could result in a similar competitive exclusion of AJ associated actin-bundling proteins α-actinin and potentially EPLIN which could explain fascin1's AJ remodeling function. If true, such changes would also have significant implications for AJ mechanotransduction, because both α-actinin and EPLIN regulate AJ mechanosensitivity.[52, 53] Indeed, in *BRAF*^{V600E} Scr cells, fascin1 and α-actinin segregate to different areas of the AJ-associated actin cytoskeleton (Fig 4B). While α-actinin co-localized with the oblique contractile actin bundles of the AJs, fascin1 was associated with the actin bundles where they attach to the E-cadherin foci (Fig 4B). This close proximity of fascin1 to the E-cadherin foci also suggested to us that in *BRAF*^{V600E} CRC cells, fascin1 could play a direct role in modulating AJ mechanotransduction. As expected, in Scr cells we identified a competitive exclusion of □-actinin and EPLIN away from the AJs to the cytoplasm (Figs 4C-4D). In shF cells, the α-actinin and EPLIN distribution is restored to the cell-cell margins and the AJs similar to normal intestinal epithelial cells. Fascin1 also displaced α-actinin away from focal adhesions (FAs) of Scr cells (Supplementary Fig 2E). There was no significant difference in total α-actinin protein levels between control and fascin1 KD HT-29/19A cells (Supplementary Fig 2E). To quantitatively measure the effects of fascin1 on AJ actin dynamics, we transfected HT-29/19A-Scr and shF cells with mCherry-Lifeact (Fig 4E). As anticipated, kymographs revealed greater movement and greater velocity of movement of F-actin at the AJs of Scr

cells compared to shF cells indicative of greater AJ plasticity. In normal epithelial cells, α-catenin is a key mechanosensor and monomeric α-catenin (α^M) couples the E-cadherin-β-catenin complex to the actin cytoskeleton and recruits vinculin to reinforce the AJ stability while the α-catenin that dissociates from the cadherin-catenin complex homodimerizes (α^D).[54-56] In this manner α-catenin and vinculin function as major mechanosensors that transmit the force of actomyosin contraction to the E-cadherin-β-catenin complex.[57-59] To directly measure the effect of fascin1 KD on AJ mechanotransduction, we evaluated the association of vinculin with the AJs and the association of vinculin with α-catenin.[56] While significant displacement of vinculin away from AJs (apical) and FAs (basal) to the cytoplasm was observed in HT-29/19A-Scr cells, fascin1 KD in HT-29/19A-shF cells restored vinculin localization to these cell adhesion sites similar to vinculin's distribution in normal epithelial cells (Fig 4F; Supplementary Fig 2E).[60] There was no significant difference in total vinculin protein levels between Scr and shF cells (Supplementary Fig 2E). Quantitative co-immunoprecipitation (IP) assay with an antibody that specifically immunoprecipitates monomeric α-catenin revealed that fascin1 knockdown also resulted in higher levels of vinculin in complex with α-catenin (Fig 4F). Together these data show that by simply competing with other actin-bundling proteins fascin1 reorganizes cellular actin cytoskeleton and remodels the AJs by displacing key AJ mechanosensors. Previously, such phenotypic changes in CRC cells have been linked to BRAF^{V600E} mutation.[21-23]

Fascin1 activates Wnt signaling which correlates with increased proliferation and dedifferentiation of BRAF^{V600E} CRC cells: Wnt activation in response to changes in AJ

mechanotransduction plays an important role during morphogenesis and in tumorigenesis when these conserved embryonic mechanosensitive pathways are reactivated in the adult tissue.[57, 61] We reasoned that by remodeling *BRAF*^{V600E} CRC cell AJ mechanotransduction, fascin1 could drive oncogenic Wnt activation. Indeed, subcellular fractionation showed that fascin1 KD significantly inhibited the nuclear accumulation of β-catenin (60.2%, n=3, $p<0.001$), and caused a redistribution of β-catenin from the nucleus and cytoplasm to the cell-cell margins and the AJs without impacting total β-catenin or E-cadherin protein levels (Fig 5A, Supplementary Figs 3A). Most notably, re-expression of EGFP-Fascin1 in the fascin1 KD shF cells resulted in the redistribution of β-catenin from the cell-cell margins and AJs back to the nucleus (Fig 5A) validating fascin1's direct role in nuclear accumulation of β-catenin. Actively invading Scr cell tumor spheroids confirmed significant nuclear accumulation of β-catenin (Fig 5B). Nuclear accumulation of β-catenin was also identified in MDCK cells overexpressing EGFP-Fascin1 further validating the role of AJ mechanotransduction in fascin1-mediated Wnt activation (Supplementary Fig 3B). Likewise in the CRC patient cohort high fascin1 protein expression (score 2-3) was associated with widespread (score 2) accumulation of nuclear β-catenin validating the pathophysiological significance of this function of fascin1 (Fig 5C). Fascin1 KD in mutant *BRAF*^{V600E} CRC cells also resulted in reduced expression of Wnt target genes including the marker for stemness, *Cd44,* the ECM remodeling proteins, matrix metalloproteinase, *Mmp7*and *Mmp9* and more importantly, *c-Myc* which has been shown previously to reverse the growth inhibitory effects of mutant BRAF^{V600E} (Fig 5D).[18] Reduced Wnt activation was confirmed by chromatin immunoprecipitation (ChIP-PCR) assay with the β-catenin antibody (Supplementary Fig 3C). Fascin1's

function as a driver of Wnt activation was validated with the Super8x TOP-Flash luciferase TCF-LEF reporter assay (Supplementary Fig 3D). The reduction of Wnt activation induced by fascin1 KD was also accompanied by significant changes in cell morphology and cell behavior such as reduced anchorage-independent growth (Fig 5E), restoration of TJ morphology (Fig 5F), and restoration of contact inhibition (Fig 5F). Loss of contact inhibition was phenocopied in the rescue experiments performed in fascin1 KD shF cells overexpressing EGFP-Fascin1 cells (Supplementary Fig 4A) and in gain-of-function studies performed in MDCK cells overexpressing EGFP-Fascin1 (Supplementary Fig 4B). Additionally, fascin1 KD in the *KRAS* mutant and wild type *BRAF* expressing HCT-116 cells restored contact inhibition indicating that fascin1's AJ remodeling function may be recapitulated in SCRCs with KRAS mutation (Supplementary Figs 4C).[62 21] Together, our studies demonstrate that by activating Wnt target genes fascin1 plays a direct role in restoring oncogenic cell behavior in mutant BRAF^{V600E} CRC cells.

Fascin1 activates Wnt signaling in BRAF^{V600E} mutant CRC cells to accelerate primary and secondary tumor growth. We reasoned that by activating Wnt target genes that promote cell proliferation and cell migration/invasion fascin1 could accelerate BRAF^{V600E}-driven tumorigenesis. To test this idea, we assessed the effects of fascin1 KD on primary and secondary tumor growth of *BRAF^{V600E}* mutant CRC cells *in vivo*. Fascin1 KD significantly reduced primary tumor weight compared to control cells (Fig 6A; $p<0.01$, $n=6$) and reduced the number of actively proliferating tumor cells validating fascin1's role in the etiology of BRAF^{V600E} driven CRCs (Supplementary Fig 5A). More importantly, fascin1 KD induced a re-localization of total and active (NP) β-catenin from the nucleus

and cytoplasm to the cell membrane (Figs 6B-6C, respectively). We used the active (NP) β-catenin antibody to demonstrate the presence of active cytoplasmic β-catenin in these tumors. Most remarkably, in this *in vivo* model system, we validate fascin1's AJ remodeling function by identifying ultra-long TM-like cell-cell junctions within the primary tumor (Fig 6D). Fascin1 KD significantly reduced secondary tumor growth in mice (Fig 6E; $p<0.01$, $n=8$) and prevented the cytoplasmic and nuclear accumulation of total and active β-catenin (Fig 6E). Fascin1 KD also reduced CRC cell metastasis in a zebrafish embryo metastasis assay (Supplementary Fig 5B) validating this as a conserved function of fascin1. These data demonstrate that Wnt activation regulated by fascin1 cooperates with the oncogene $BRAF^{V600E}$ to accelerate and augment tumor growth and metastasis.

In CRCs fascin1 expression is linked to the E/M metastable state. Since fascin1 remodels AJ mechanotransduction, we postulated that fascin1 upregulation in CRCs could also influence signals regulating epithelial-to-mesenchymal transition (EMT). More recently, fascin1 overexpression in epithelial ovarian cancers has been linked to increased SNAI1 levels suggesting fascin1 upregulation could have a direct effect on EMT.[63] For this we analyzed RNA-Seq data from CRCs profiled by the TCGA consortium, which revealed a significant inverse correlation between mRNA expression of fascin1 and the epithelial phenotype stability factors (PSFs) *OVOL1* and *GRHL2* (Fig 7A) and conversely, a significant positive correlation with the metastable markers *SNAI1/2/3*.[64] The modest inverse correlation of fascin1 with *OVOL* and *GRHL2* suggests dampening of epithelial characteristics but not complete EMT and the positive correlation with *SNAI* suggests stabilization of the E/M state. We also identified a significant positive correlation

between fascin1 and *ZEB1/2* expression. Since stromal cells (e.g. fibroblasts) also express fascin1 and *ZEB1/2* proteins, we also performed these analyses in RNA-Seq data obtained from 61 CRC cell lines, which revealed similar findings confirming these changes were tumor intrinsic (Fig 7B). These data are consistent with fascin1's function in CRC cell AJ remodeling.

Fascin1 increases the rate of cell migration and generates bidirectional cell migration. As collective cell migration is a hallmark of the hybrid E/M metastable state we assessed the role of fascin1 in a wound-closure assay. Intestinal epithelial cells move collectively as closely adherent sheet of migrating cells. As expected, EGFP expressing MDCK cells migrated as a sheet of tightly adherent cells very similar to normal intestinal epithelial cells (Supplementary Videos 3-4; Fig 7C). As predicted, fascin1 overexpression significantly increased cell migration rates compared to control cells. Unlike control cells, Fascin1 expressing cells migrated as loosely adherent group of cells. We identified three groups of migrating EGFP-Fascin1 cells that we refer to as loose, edge and bulk, which migrated at different speeds and with different patterns (Supplementary Video 3-4; Supplementary Table 1; Figs 7D-7E). Loose and edge cells migrated using TM-like structures connecting the back of a leading cell with the front of a follower cell (Supplementary Videos 3-4, Supplementary Fig 6A). By measuring the area of migrating bulk cells, it is clear that migrating bulk cells also remodel cell-cell adhesions (Supplementary Videos 3 and 4; Supplementary Fig 6B). Migrating EGFP-Fascin1 cells displayed large gaps within the migrating cell clusters, indicative of increased tension at cell-cell adhesion sites and continuous AJ remodeling during cell migration

(Supplementary Videos 3 and 4; Supplementary Fig 6D). These data demonstrate that fascin1's AJ remodeling property also influences the behavior of collectively migrating epithelial cells. Additionally, we made the most striking finding that fascin1 overexpressing loose cells displayed significantly more backwards migration events in the direction opposite from the wound edge, which were quantitatively measured by the shape metrics (Supplementary Video 4; Figs 7D-7E, Supplementary Fig 6C, Supplementary Table 2). Based on the analysis of X and XY (radial) coordinates, the backwards migration of EGFP-Fascin1 cells was significantly different from the consistent forward migration of control EGFP cells. To the best of our knowledge fascin1's role in bidirectional migration has not been reported before. Villin1 is an actin bundling protein that assembles filopodia and increases intestinal cell migration rates during normal intestinal wound repair.[65, 66] MDCK cells overexpressing EGFP-Villin1 migrated unidirectionally as a sheet of tightly adherent cells resembling normal intestinal epithelial cell migration, demonstrating the unique ability of fascin1 to produce bidirectional cell migration (Supplementary Video 5). Together these data demonstrate that fascin1 expression in epithelial cells increase rates of cell migration and endows cells with the ability to migrate bidirectionally. Additionally, these data demonstrate that fascin1's AJ remodeling property also influences its function in cell migration.

Conclusions

Multiple studies have shown that while the $BRAF^{V600E}$ oncogene is a prevalent driver of human cancers, it is inefficient in promoting tumorigenesis in animal models of cancer.[16, 67] In the intestine, ectopic expression of $BRAF^{V600E}$ induces senescence,

differentiation of intestinal stem cells, or p21 expression. [11, 14-16] Previous studies have also shown that inducing dedifferentiation or restoring Wnt signaling stimulates BRAF^{V600E}-driven tumorigenesis.[11, 13, 18, 23, 68, 69] Elevated Wnt signaling is also common to both the genetic mouse models of BRAF^{V600E}-driven SCRC.[11] Consistent with that precursor intestinal lesions with BRAF^{V600E} mutation progress to cytologic dysplasia only after they acquire Wnt pathway activity.[10, 70, 71] SSLs and serrated pathway CRCs lack inactivation mutations in Apc or Wnt pathway genes.[2, 9] Despite the suggestion, serrated pathway CRCs lack methylation of Wnt pathway genes.[72] Therefore, the molecular mechanism regulating Wnt activation in BRAF^{V600E}-driven carcinogenesis has remained unresolved. Fascin1 is upregulated early in SSLs and our data show fascin1's direct role in Wnt activation suggesting a role for fascin1 in the initiation of serrated pathway carcinogenesis.[2, 35-37] Fascin1 upregulation in SCRCs driven by mutant BRAF also suggests that fascin1 regulated Wnt signaling also cooperates with the BRAF oncogene to regulate the progression of serrated pathway tumors.[21] We propose that by coordinating oncogenic Wnt activation with BRAF^{V600E} activation fascin1 regulates both the initiation and progression of SCRCs. This is supported by our finding that fascin1 KD in mutant BRAF CRC cells impairs tumor growth and metastasis in mice due to loss of Wnt activation. Conditional overexpression of fascin1 in mouse intestine does not induce tumor formation and fascin1 is not an oncogene.[73] Based on that, we propose that fascin1 plays a key role in serrated pathway carcinogenesis by generating a cooperating signaling pathway that reverses BRAF^{V600E}-induced senescence and differentiation to accelerate tumor growth and metastasis. By activating Wnt signaling fascin1 renders colon epithelial cells responsive to the oncogene BRAF^{V600E}. This idea is supported by the finding that

the ability of HT-29 cells, which express BRAF^{V600E} but no fascin1, to form metastatic lesions in the lung when injected in mouse tail vein is negligible but is enhanced 10 times when fascin1 is ectopically overexpressed in these cells.[30] A role for fascin1 in colorectal tumor initiation has been shown previously by constitutive overexpression of fascin1 in the intestinal epithelium in the *Apc*-mutated mouse background where fascin1 expression also increased accelerated tumor progression, increased tumor invasion and decreased mouse survival.[73] Mechanical cues can initiate tumor-like gene expression pattern in pre-neoplastic tissues of the *Apc* mutant mice, this could explain why conditional expression of fascin1 in mutant Apc mice promotes tumor initiation.[61] This study also lends support to our idea that fascin1 upregulation in the presence of oncogenes drives colorectal tumorigenesis. We show that fascin1 upregulation in BRAF^{V600E} mutant CRC cells is linked to activation of Wnt target gene c-Myc. Upregulation of c-Myc has been correlated with malignant transformation in the serrated pathway CRCs.[74] c-Myc overexpression is also required for continuous suppression of BRAF^{V600E}-induced senescence and differentiation to induce tumorigenesis in animal models of human cancers.[75] [18, 76, 77] *In vitro* studies using BRAF inhibitors and transcriptomic analysis of mutant BRAF CRC cell lines have identified fascin1 as a key gene regulating dedifferentiation of mutant BRAF CRC cells.[22] Previously, it has been shown that inducing dedifferentiation surmounts BRAF^{V600E}-induced senescence to accelerate serrated pathway carcinogenesis in mice.[11] Here, we show that fascin1 is more highly expressed in high grade/poorly differentiated CRCs. Together, these findings point to a role for fascin1 in dedifferentiation of serrated pathway tumors as a mechanism to increase intestinal susceptibility to BRAF^{V600E}. Taken

together our findings demonstrate that fascin1 expression in SCRCs creates the conditions necessary for BRAF^{V600E}-driven tumor initiation and progression.

Little is known about the molecular events that drive serrated pathway carcinogenesis however, there is sufficient evidence that *BRAF^{V600E}* mutation correlates with major cytoskeletal reorganization and remodeling of cell-cell adhesions both AJs and TJs.[21, 22] In this study we provide a molecular mechanism for these cellular changes and identify fascin1 as a major driver of these changes. Our data show that in *BRAF^{V600E}* CRC cells, cytoskeletal reorganization, AJ and TJ remodeling are phenocopied by fascin1. It is known that fascin1 and α-actinin form actin bundles with very different inter-filament spacing, 8 nm *versus* 35 nm, respectively.[51] We propose that in *BRAF^{V600E}* CRC cells, the tightly packed actin bundles formed by fascin1 exclude non-muscle myosin II (NMII) which is revealed by the absence of fascin1 from the contractile actin bundles of the AJs. We suggest that this is likely the mechanism that displaces α-actinin and EPLIN from the AJs. It is also known that both fascin1 and α-actinin assemble stable cross-linked actin networks but when these two structures are mixed together they form unstable structures because α-actinin crosslinks impose unfavorable and energetically costly defects in hexagonally packed structures formed by fascin1 and *vice versa*.[78] We propose that such energetically costly defects caused by fascin1 expression in *BRAF^{V600E}* CRC cells could provide the mechanism responsible for increased AJ actin dynamics and increased AJ plasticity seen in fascin1 expressing cells during cell migration. In the absence of Wnt ligands, mechanical forces that change AJ mechanotransduction are sufficient to promote nuclear accumulation of β-catenin to drive Wnt target genes, and in this fashion they can induce mechanical-strain induced changes in epithelial cell behavior.[79] In the quiescent

epithelium, mechanical strain is sufficient to activate β-catenin and cell cycle re-entry.[57, 79, 80] We propose that the profound changes in AJ actin cytoskeleton and AJ mechanotransduction that are induced in response to fascin1 expression are sufficient for aberrant Wnt activation in the mutant BRAF^{V600E} CRC cells. One previous study has shown that in CRC cells fascin1 is itself a target of β-catenin-TCF signaling.[30] While we did not see a similar effect of Wnt signaling on fascin1 expression, a feedback mechanism between Wnt and fascin1 is possible. Targeted Wnt therapies for the treatment of CRCs have been unsuccessful due to the pleiotropic effects of Wnt. Most of these drugs also target ligand-receptor Wnt signaling, a likely factor in their ineffectiveness. The fascin1 knockout mice do not have any major defects, and since fascin1 is absent from the normal colon, we propose that fascin1 is a potential therapeutic target to prevent oncogenic Wnt activation in the serrated pathway CRCs. In this study, we also identify for the first time, the ability of fascin1 to assemble TM-like ultra-long, large and long-lived cell-cell connections. We show that these TM-like structures contain E-cadherin and β-catenin, which suggests that the origins of these structures are similar to epithelial protrusions that assemble and/or repair AJs in normal intestinal epithelial cells.[81] These findings also indicate that fascin1 appropriates this molecular machinery to construct TM-like junctions. We show that in *BRAF*^{V600E} CRC cells these super-elongated cell-cell junctions share many structural and functional similarities with TNTs, neuronal growth cones and TMs such as their morphology, their inclusion of tubulin and organelles, and their ability to hover over cell surfaces while connecting distant cells.[43, 44] TNTs are understood to correspond to invadopodia *in vivo* and TMs *in vivo* have been shown to regulate tumor cell migration/invasion but also tumor proliferation and radioresistance.[44, 82] While these

TM-like structures remain to be identified in serrated pathway CRCs, we hypothesize that this property of fascin1 also implicates it in SCRC cell invasion and chemoresistance. These TM-like intercellular connections could have other functions e.g. as conduits for cell signaling allowing cells at the invasive front and the tumor center to communicate directly, or to function like cytonemes to traffic morphogens and generate morphogen gradients. Since stromal cells also expression fascin1, morphogen trafficking between the stromal and tumor cells can be envisioned and could influence CRC tumor heterogeneity. Tumor heterogeneity is responsible for the failure of most cancer therapies and this may be the molecular basis for fascin1's strong association with treatment-refractory SCRCs.

The expression of TFs such as *OVOL* and *ZEB* and *OVOL* and *SNAI* induce the hybrid E/M metastable state.[83] We find that fascin1 expression in CRCs is linked to the hybrid E/M state which is consistent with its role in AJ remodeling. While we predict that the majority of carcinomas expressing fascin1 will have an E/M phenotype, some fascin1 expressing cancers could reflect a complete phenotypic transition to M due to rewiring of EMT regulatory networks and/or differences in epigenetic reprogramming. Our cell migration studies demonstrate that fascin1 expressing cells migrate collectively using TM-like remodeled cell-cell connections which could function *in vivo* as guidance cues. This is supported by the knowledge that similar AJ elongation during morphogenesis provides directional cues to the migrating cells.[84] We also interpret this as reactivation of embryonic cell migration patterns in $BRAF^{V600E}$-mutated CRCs, and this may be a recapitulation of fascin1's function in the developing gut. Such patterns of cell migration are not seen during normal intestinal wound healing and are not duplicated by villin1. These TM-like structures could provide $BRAF^{V600E}$-driven tumor cells with an advantage when

responding to external cues by rapidly remodeling AJs allowing CRC cells to switch between more closely or more loosely adherent cells as they navigate their way through the underlying tissue to achieve successful metastasis.[65] Bidirectional migration of leukocyte T cells and vertebrate axon growth cones is regulated by chemoattraction and chemorepulsion.[85, 86] It is noteworthy that growth cones express fascin1 and fascin1 regulate growth cone motility during neuronal synaptogenesis.[87] Fascin1 could recapitulate this function in SCRCs and bidirectional migration could enhance the response of *BRAF*^{V600E}-driven tumor cells to both chemoattractants and chemorepellents which would also promote tumor metastasis. It is clear that other intestinal actin crosslinking proteins like villin1 lack this function which may explain why fascin1 is re-expressed in metastatic CRCs. In summary, we provide for the first time, a functional characterization of fascin1 in serrated neoplasia pathway and identify fascin1's novel role in this pathway that contributes to tumor growth and metastasis. Our study provides a molecular mechanism for oncogenic Wnt activation in serrated pathway CRCs and identifies a role for fascin1 in creating conditions in the intestinal cells that favor BRAF^{V600E}-driver carcinogenesis. We postulate that targeting fascin1's function in AJ remodeling could provide a novel, effective therapeutic approach to treat SCRCs.

Figure Legends

Figure 1. The role of fascin1 in CRC with BRAF^{V600E} mutation. **(A)** CRCs were graded for fascin1 protein expression and pie chart show the correlation of fascin1 with CRCs. **(B)** Fascin1expression increases significantly with increasing tumor grade (G1>G2>G3, **p<0.01, n=270). **(C)** Phase contrast image of HT-29/19A-Scr and shF cells grown as suspension 48 h tumor spheroids. Scale bar, 25 µm. **(D)** Confocal images of sub confluent HT-29/19A-Scr and HT-29/19A-shF cells show distribution of actin (red) and tubulin. Nuclei were counter stained with DAPI. Scale bar, 50 µm (Scr) and 10 µm (shF). **(E)** Confocal image of sub confluent HT-29/19A-Scr cells shows distribution of actin (magenta), tubulin (red), and fascin1 (green). Nuclei were counter stained with DAPI. Scale bar, 30 µm. **(F)** Confocal image of HT-29/19A-Scr cells shows distribution of actin (red), tubulin (cyan) and E-cadherin (green). Nuclei were counter stained with DAPI. Scale, 10 µm.

Figure 2. In CRC cells with BRAFV600E mutation fascin1 remodels AJ assembly. **(A)** Confocal image of Scr and shF cells shows distribution of actin (green), E-cadherin (red) and β-catenin (cyan) as two cells (cell 1 and 2) assemble nAJs. Arrowheads identify, oblique actin bundles, E-cadherin and β-catenin foci (white). Elongated nascent cell-cell junctions with or without distal lamellipodia (cyan). Right panel is a magnification of the boxed area. Scale, 20 µm. **(B)** Confocal image of MDCK EGFP-Fascin1 cells shows distribution of fascin1 (green) and E-cadherin (red). Scale bar, 20 µm. **(C)** Confocal image of MDCK EGFP-Fascin1 cells shows the distribution of fascin1 (green) and β-catenin

(red) during nAJ assembly. Bottom panels are magnification of the boxed areas shown above. Scale bar, 10 µm. **(D)** Confocal image MDCK EGFP-Fascin1 cells shows growth-cone like cellular protrusion during nAJ assembly. Scale bar, 20 µm. **(E)** Live confocal immunofluorescence of MDCK EGFP-Fascin1 cells labeled with MitoTracker-Red and LysoTracker Red show the presence of functional mitochondria and lysosomes in these elongated nascent AJs. Asterisks highlight mitochondria and lysosomes, respectively. Scale bar, 10 µm.

Figure 3: Fascin1 remodels mature AJs and assembles ultra-long, large and long-lived tumor microtube-like intercellular connections. (A) Confocal immunofluorescence z-stacks (xy images;1 µm each from (a) to (f)) show the distribution of fascin1 (green) and actin (red) in confluent MDCK EGFP-Fascin1 cells. Arrowhead identifies TM-like intercellular junctions connecting cell 1 to cell 6. Scale bar, 15 µm. **(B)** Live confocal immunofluorescence z stacks (xy images; 1 µm) of MDCK EGFP-Fascin1 cells show TM-like cell-cell junction suspended over the confluent monolayer. Scale bar, 25 µm. **(C)** Phase contrast images show clusters of MDCK EGFP and MDCK EGFP-Fascin1 cells at time 0 and at 17.5 h post-treatment with HGF. Scale bar, 20 µm. **(D)** Correlation of TM-like remodeled cell-cell junction length (µm) and lifespan (hrs) in HGF treated MDCK EGFP and MDCK EGFP-Fascin1.

Figure 4. Fascin1 remodels AJ mechanotransduction in CRC cells with *BRAF*^{V600E} mutation. (A) Confocal microscopy shows the distribution of actin (red) and E-cadherin (green) at the AJs (Top) and lateral junctions (Middle) of HT-29/19A-Scr and shF cells.

Nuclei were counter stained with DAPI. Plot profiles were generated by measuring the distribution of actin and E-cadherin in ROI highlighted by a white line, 10 μm long. Scale, 10 μm. **(B)** Virtual Channel confocal microscopy shows the AJ associated actin (red), fascin1 (green) and α-actinin (cyan) in Scr cells. Scale bar, 10 μm. **(C)** Confocal immunofluorescence of HT-29/19A-Scr and shF cells show the distribution of E-cadherin (green) and α-actinin (red) at the AJs. Nuclei were counter stained with DAPI. Plot profiles were generated by measuring the distribution of E-cadherin and α-actinin in ROI highlighted by a white line, 10 μm long. Scale bar, 10 μm. **(D)** Virtual Channel confocal immunofluorescence of HT-29/19A-Scr and shF cells shows distribution of actin (red), E-cadherin (cyan), and EPLIN (green) at the AJs. Nuclei were counter stained with DAPI. Plot profiles were generated by measuring the distribution of EPLIN and actin in ROI highlighted by a white line, 10 μm long. Scale bar, 10 μm. **(E)** Live cell imaging of HT-29/19A-Scr and shF cells stably expressing mCherry-Lifeact. Nuclei were counter stained with Hoechst. Scale bar, 5μm. Kymograph analysis of mCherry-Lifeact at AJs of Scr and shF cells measured at two ROI (labeled 1 and 2, 10 μm each) shows difference in speed (μm/min) of migration and distance (μm/min) moved by AJ-associated F-actin in Scr and shF cells. Asterisk (****) denotes $p<0.001$, $n=6$. **(F)** Confocal images of Scr and shF cells show xz distribution of vinculin (green) and actin (red). Nuclei were counter stained with DAPI. Scale bar, 10 μm. Accumulation of cytoplasmic vinculin in Scr and shF cells was measured from three independent experiments (***) denotes $p<0.001$, $n=3$. Scr and shF cell lysates were immunoprecipitated with α-catenin antibody and immunoblotted with vinculin antibodies. Asterisks (*) denote as follows: *** denotes $p<0.001$, $n=3$ and **** $p<0.0001$, $n=3$.

Figure 5. Fascin1 activates Wnt signaling in CRC cells with BRAF^{V600E} mutation. (A) Confocal immunofluorescence of HT-29/19A-Scr, shF and shF expressing Fascin1 shows the distribution of total β-catenin (green). Nuclei were counter stained with DAPI. Scale bar, 10 μm. Subcellular fractionation assays were performed to quantify the distribution of β-catenin in the nuclear (N), cytoplasmic (C) and whole cell (WC) lysate fractions. Asterisk (****) denotes $p<0.0001$, n=3. **(B)** Phase contrast image shows actively invading Scr cell tumor spheroids at day 0 and at the end of day 8. Confocal images show the distribution of fascin1 (green) and β-catenin (red) in actively invading Scr cell tumor spheroids. Nuclei were counter stained with DAPI. Right panels (i) and (ii) are magnifications of the boxed areas labelled (i) and (ii). **(C)** Immunohistochemistry in paired panels show fascin1 and widespread nuclear β-catenin accumulation in the same colorectal tumor. Arrowheads highlight widespread accumulation of nuclear β-catenin in high fascin1 expressing tumors. **(D)** Quantitative RT-PCR for Wnt target genes using total cellular mRNA extracted from Scr and shF cells. Asterisks (*) denote as follows: * $p<0.05$, ** $p<0.01$, *** $p<0.001$ (n=6). **(E)** Phase contrast image of anchorage-independent colonies of HT-29/19A-Scr and shF cells. Asterisk (*) denotes $p<0.05$, n=3. **(F)** Confocal immunofluorescence shows xz distribution of ZO-1 (green) and actin (red) (left panels) and xz distribution of actin (red) and Ki67 (green; right panels) in Scr and shF cells. Nuclei were counter stained with DAPI. Asterisk (***) denotes $p<0.001$, n=3.

Figure 6. Fascin1's function in Wnt signaling cooperates with the oncogene BRAF^{V600E} to accelerate primary and secondary tumor growth in mice. (A) IVIS imaging of NSG mice injected subcutaneously with *BRAF^{V600E}* mutant HT-29/19A-Scr and

shF cells. Fascin1 KD significantly decreased primary tumor weight. Asterisk (**) denotes p<0.001, n=6. **(B)** Confocal immunofluorescence shows distribution of total β-catenin in primary tumors of mice injected with Scr and shF cells. Nuclei were counter stained with DAPI. Scale bar, 10 μm. **(C)** Immunohistochemistry shows distribution of active (NP) β-catenin in primary tumors from mice injected with *BRAF*^{V600E} mutant HT-29/19A-Scr or shF cells. Yellow arrowheads label nuclear accumulation of active β-catenin. **(D)** Confocal image of primary tumor from Scr injected mice shows TM like remodeled AJs and the distribution of actin (red) and fascin1 (green) in these remodeled cell-cell junctions (arrowhead). Nuclei were counter stained with DAPI. Right panel is a magnification of the boxed area. **(E)** Secondary tumor growth in liver of mice injected with Scr or shF cells. Asterisk (**) denotes p<0.0.001, n=8. Immunohistochemistry of secondary tumors from mice injected with Scr and shF cells shows distribution of fascin1, total β-catenin and active (NP) β-catenin in tumor (T) and surrounding normal (N) tissue. White arrowheads identify nuclear accumulation of β-catenin.

Figure 7. Fascin1 expression in CRCs correlates with a hybrid E/M metastable state. (A-B) Correlation analysis of mRNA expression levels of fascin1 with epithelial (*OVOL1*, *OVOL2* and *GRHL2*), mesenchymal (*ZEB1* and *ZEB2*), and E/M stability markers (*SNAIL1*, *SNAIL2*, *SNAIL3*) in **(A)** CRCs, n=273, and **(B)** CRC cell lines, n=61. **(C)** Phase contrast image of scratch wound of MDCK control cells expressing EGFP or overexpressing EGFP-Fascin1. Cells identified by our tracking method are shown in green (bulk), red (edge) or blue (loose). Scale bar, 50 μm. See methods for description of group classifications. Quantification of instantaneous migration speeds are shown as

mean ($\bar{x}$) ± SD. P-value from Mann-Whitney U test comparing MDCK EGFP and MDCK EGFP-Fascin1 cells. **(D)** Quantification of instantaneous migration velocity in X coordinates only and in XY-radial coordinates. Instantaneous migration velocity frequencies in XY-radial coordinates. **(E)** Instantaneous velocity-angle histograms of migrating MDCK EGFP and MDCK EGFP-Fascin1 bulk, edge, and loose cell clusters.

Supplementary Figure 1. (A) Endogenous fascin1 expression in HT-29/19A-Scr and HT-29/19A-shF cells and ectopic overexpression of EGFP-Fascin1 in HT-29/19A-shF cells. Tubulin was used as a loading control. This immunoblot is a representative of at least three independent experiments with similar findings. **(B)** Confocal immunofluorescence shows distribution of F-actin (red), tubulin (green) and fascin1 (magenta) in nAJs of Scr cells. Nuclei were counter stained with DAPI. Scale bar, 30 μm. **(C)** Phase contrast image of HT-29/19A-Scr and shF cells. Scale bar, 10 μm. Rate of elongated nAJ assembly was measured in HT-29/19A-Scr and shF cells. Data are presented as mean ± S.E.M.; Student's t-test. Asterisk (***) denotes $p<0.001$, n=10 fields/group and >300 cells/group. **(D)** Phase contrast image of HT-29/19A-Scr cells. Scale bar, 10 μm. Rate of elongated nAJ assembly was measured in Scr cells 48 h post-treatment with vehicle control (DMSO), cytochalasin B (250 nM), or colchicine (1 mM). Data are presented as mean ± S.E.M.; Students's t-test. Asterisk (***) denotes $p<0.001$, n=10 fields/group and >300 cells/group. Asterisk (****) denotes $p<0.0001$, n=10 fields/group and >300 cells/group. **(E)** Ectopic overexpression of EGFP-Fascin1 in MDCK cells. Tubulin was used as a loading control.

Supplementary Figure 2. (A) Immunoblot shows ectopic overexpression of EGFP and EGFP-fascin1 in HT-29 cells, a *BRAF*^{V600E} CRC cell line that lacks endogenous fascin1 protein. Tubulin was used as a loading control. This immunoblot is a representative of at least three independent experiments with similar findings. **(B)** Confocal immunofluorescence of HT-29 EGFP and HT-29 EGFP-Fascin1 cells shows distribution of AJ associated actin (red) and EGFP (green). Nuclei were counter stained with DAPI. Scale bar, 10 μm. **(C)** Confocal image of MDCK EGFP and MDCK EGFP-Fascin1 cells shows distribution of AJ associated actin (red) and EGFP (green). Nuclei were counter stained with DAPI. Scale bar, 10 μm. **(D)** Confocal image of shF cells overexpressing EGFP or EGFP-Fascin1 shows distribution of AJ associated actin (red) and EGFP (green). Scale bar, 10 μm. **(E)** Confocal image shows the distribution of focal adhesion associated actin (red), α-actinin (green) and vinculin (green) in Scr and shF cells. Right panels are magnifications of the boxed areas. Immunoblot shows total vinculin, fascin1 and α–actinin levels in Scr and shF cells. Tubulin was used as a loading control. This immunoblot is a representative of at least three independent experiments with similar findings.

Supplementary Figure 3. (A) Immunoblot shows total E-cadherin and β-catenin levels in Scr and shF cells. Tubulin was used as a loading control. This immunoblot is a representative of at least three independent experiments with similar findings. **(B)** Confocal immunofluorescence z-stack of MDCK EGFP-Fascin1 cells shows distribution of fascin1 and β-catenin. Nuclei were counter stained with DAPI. Scale bar, 20 μm. Data obtained from n = 10 fields/group, and >15 cells/group. (**C)** ChIP-qPCR with β-catenin

antibody and cell lysates from HT-29/19A-Scr and shF cells. ChIP with IgG and negative control primers against a region of MMP9 were used as control. Data are representative of n=3 biological replicates, mean ± S.E.M.; Student's t-test. Asterisk (*) denotes *p<0.05, n=3. NS, not significant, **(D)** Wnt signaling activity in *BRAF*^{V600E} mutant HT-29/19A-Scr and shF cells was monitored using TOP Flash luciferase reporter assay. Data are shown as mean ± S.E.M., Student's t-test. Asterisk (*) denotes p<0.01, n=3.

Supplementary Figure 4. (A) Confocal image of shF EGFP and shF EGFP-Fascin1 cells shows xz distribution of actin (red) and EGFP (green). Nuclei were counter stained with DAPI. Scale bar, 10 μm. **(B)** Confocal image of MDCK EGFP and MDCK EGFP-Fascin1 cells shows xz distribution of actin (red) and EGFP (green). Nuclei were counter stained with DAPI. Scale bar, 10 μm. **(C)** Confocal image shows xz distribution of actin (red) in HCT-116 expressing scrambled shRNAs (Scr) and HCT-116 cells transduced with shRNAs to KD fascin1 (shF cells). Nuclei were counter stained with DAPI. Scale bar, 10 μm. Immunoblot shows total fascin1 levels in HCT-116 cells expressing scrambled shRNA (Scr) and HCT-116 with fascin1 KD using fascin1 specific shRNA (shF). Actin was used as a loading control. This immunoblot is a representative of at least three independent experiments with similar findings.

Supplementary figure 5. (A) Confocal immunofluorescence of primary tumors from mice injected with Scr or shF cells labeled for cell proliferation (Ki67, green) and apoptosis (cleaved caspase-3, red). Nuclei were counter stained with DAPI. Scale bar, 10 μm. **(B)** Scr and shF cells labeled with dye (red) injected into 2-day old zebrafish embryos and

metastasis scored for 72 h post-injection. This is a representative of three independent experiments with similar findings. **(C)** Analysis of mRNA expression levels of fascin1; (*OVOL1* and *GRHL2*), mesenchymal (*ZEB1* and *ZEB2*), and E/M stability markers (*SNAIL1*, *SNAIL2*, *SNAIL3*) in intestinal tumors and normal intestinal tissue from mutant *Apc* mice. Asterisks denote the following: **p<0.001, n=5 and ****p<0.0001, n=5.

Supplementary figure 6 (A) Phase contrast microscopy shows TM-like long intercellular junction connecting two migrating MDCK EGFP-Fascin1 loose cells. Arrowheads indicates the TM-like structure. **(B)** Total area (μm^2) covered by 'bulk' cells was measured in migrating MDCK EGFP and MDCK EGFP-Fascin1 cells. Asterisk (****) denotes p<0.0001, n=3. **(C)** Time lapse phase contrast imaging of MDCK EGFP-Fascin1cells captured every 10 min. Start time, 20.30 and finish time, 1:02:40 **(D)** Large gaps (arrowheads) identified in migrating MDCK EGFP-Fascin1 cells.

References Cited

1. De Sousa EMF, Wang X, Jansen M, et al. Poor-prognosis colon cancer is defined by a molecularly distinct subtype and develops from serrated precursor lesions. Nat Med 2013;19:614-8.
2. Chen B, Scurrah CR, McKinley ET, et al. Differential pre-malignant programs and microenvironment chart distinct paths to malignancy in human colorectal polyps. Cell 2021;184:6262-6280 e26.
3. Pai RK, Jayachandran P, Koong AC, et al. BRAF-mutated, microsatellite-stable adenocarcinoma of the proximal colon: an aggressive adenocarcinoma with poor survival, mucinous differentiation, and adverse morphologic features. Am J Surg Pathol 2012;36:744-52.
4. Kopetz S, Grothey A, Yaeger R, et al. Encorafenib, Binimetinib, and Cetuximab in BRAF V600E-Mutated Colorectal Cancer. N Engl J Med 2019;381:1632-1643.
5. Kopetz S, Desai J, Chan E, et al. Phase II Pilot Study of Vemurafenib in Patients With Metastatic BRAF-Mutated Colorectal Cancer. J Clin Oncol 2015;33:4032-8.
6. Karapetis CS, Jonker D, Daneshmand M, et al. PIK3CA, BRAF, and PTEN status and benefit from cetuximab in the treatment of advanced colorectal cancer--results from NCIC CTG/AGITG CO.17. Clin Cancer Res 2014;20:744-53.
7. Pietrantonio F, Petrelli F, Coinu A, et al. Predictive role of BRAF mutations in patients with advanced colorectal cancer receiving cetuximab and panitumumab: a meta-analysis. Eur J Cancer 2015;51:587-94.
8. Modest DP, Martens UM, Riera-Knorrenschild J, et al. FOLFOXIRI Plus Panitumumab As First-Line Treatment of RAS Wild-Type Metastatic Colorectal

Cancer: The Randomized, Open-Label, Phase II VOLFI Study (AIO KRK0109). J Clin Oncol 2019;37:3401-3411.

9. Yachida S, Mudali S, Martin SA, et al. Beta-catenin nuclear labeling is a common feature of sessile serrated adenomas and correlates with early neoplastic progression after BRAF activation. Am J Surg Pathol 2009;33:1823-32.

10. Wu JM, Montgomery EA, Iacobuzio-Donahue CA. Frequent beta-catenin nuclear labeling in sessile serrated polyps of the colorectum with neoplastic potential. Am J Clin Pathol 2008;129:416-23.

11. Tong K, Pellon-Cardenas O, Sirihorachai VR, et al. Degree of Tissue Differentiation Dictates Susceptibility to BRAF-Driven Colorectal Cancer. Cell Rep 2017;21:3833-3845.

12. Anastas JN, Kulikauskas RM, Tamir T, et al. WNT5A enhances resistance of melanoma cells to targeted BRAF inhibitors. J Clin Invest 2014;124:2877-90.

13. Biechele TL, Kulikauskas RM, Toroni RA, et al. Wnt/beta-catenin signaling and AXIN1 regulate apoptosis triggered by inhibition of the mutant kinase BRAFV600E in human melanoma. Sci Signal 2012;5:ra3.

14. Carragher LA, Snell KR, Giblett SM, et al. V600EBraf induces gastrointestinal crypt senescence and promotes tumour progression through enhanced CpG methylation of p16INK4a. EMBO Mol Med 2010;2:458-71.

15. Riemer P, Sreekumar A, Reinke S, et al. Transgenic expression of oncogenic BRAF induces loss of stem cells in the mouse intestine, which is antagonized by beta-catenin activity. Oncogene 2015;34:3164-75.

16. Rad R, Cadinanos J, Rad L, et al. A genetic progression model of Braf(V600E)-induced intestinal tumorigenesis reveals targets for therapeutic intervention. Cancer Cell 2013;24:15-29.

17. Sakamoto N, Feng Y, Stolfi C, et al. BRAF(V600E) cooperates with CDX2 inactivation to promote serrated colorectal tumorigenesis. Elife 2017;6:e20331.

18. Juan J, Muraguchi T, Iezza G, et al. Diminished WNT -> beta-catenin -> c-MYC signaling is a barrier for malignant progression of BRAFV600E-induced lung tumors. Genes Dev 2014;28:561-75.

19. Campisi J. Senescent cells, tumor suppression, and organismal aging: good citizens, bad neighbors. Cell 2005;120:513-22.

20. Ou HL, Hoffmann R, Gonzalez-Lopez C, et al. Cellular senescence in cancer: from mechanisms to detection. Mol Oncol 2021;15:2634-2671.

21. Conesa-Zamora P, Garcia-Solano J, Garcia-Garcia F, et al. Expression profiling shows differential molecular pathways and provides potential new diagnostic biomarkers for colorectal serrated adenocarcinoma. Int J Cancer 2013;132:297-307.

22. Herr R, Kohler M, Andrlova H, et al. B-Raf inhibitors induce epithelial differentiation in BRAF-mutant colorectal cancer cells. Cancer Res 2015;75:216-29.

23. Reischmann N, Andrieux G, Griffin R, et al. BRAF(V600E) drives dedifferentiation in small intestinal and colonic organoids and cooperates with mutant p53 and Apc loss in transformation. Oncogene 2020;39:6053-6070.

24. Makrodouli E, Oikonomou E, Koc M, et al. BRAF and RAS oncogenes regulate Rho GTPase pathways to mediate migration and invasion properties in human colon cancer cells: a comparative study. Mol Cancer 2011;10:118.

25. De Arcangelis A, Georges-Labouesse E, Adams JC. Expression of fascin-1, the gene encoding the actin-bundling protein fascin-1, during mouse embryogenesis. Gene Expr Patterns 2004;4:637-43.

26. Zhang FR, Tao LH, Shen ZY, et al. Fascin expression in human embryonic, fetal, and normal adult tissue. J Histochem Cytochem 2008;56:193-9.

27. Hashimoto Y, Skacel M, Lavery IC, et al. Prognostic significance of fascin expression in advanced colorectal cancer: an immunohistochemical study of colorectal adenomas and adenocarcinomas. BMC Cancer 2006;6:241.

28. Shi S, Zheng HC, Zhang ZG. Roles of Fascin mRNA expression in colorectal cancer: Meta-analysis and bioinformatics analysis. Mol Clin Oncol 2020;13:119-128.

29. Tan VY, Lewis SJ, Adams JC, et al. Association of fascin-1 with mortality, disease progression and metastasis in carcinomas: a systematic review and meta-analysis. BMC Med 2013;11:52.

30. Vignjevic D, Schoumacher M, Gavert N, et al. Fascin, a novel target of beta-catenin-TCF signaling, is expressed at the invasive front of human colon cancer. Cancer Res 2007;67:6844-53.

31. Ristic B, Kopel J, Sherazi SAA, et al. Emerging Role of Fascin-1 in the Pathogenesis, Diagnosis, and Treatment of the Gastrointestinal Cancers. Cancers (Basel) 2021;13 (1):2536.

32. Tampakis A, Tampaki EC, Nonni A, et al. High fascin-1 expression in colorectal cancer identifies patients at high risk for early disease recurrence and associated mortality. BMC Cancer 2021;21:153.

33. Li A, Morton JP, Ma Y, et al. Fascin is regulated by slug, promotes progression of pancreatic cancer in mice, and is associated with patient outcomes. Gastroenterology 2014;146:1386-96 e1-17.

34. Barnawi R, Al-Khaldi S, Majed Sleiman G, et al. Fascin Is Critical for the Maintenance of Breast Cancer Stem Cell Pool Predominantly via the Activation of the Notch Self-Renewal Pathway. Stem Cells 2016;34:2799-2813.

35. Kanth P, Boylan KE, Bronner MP, et al. Molecular Biomarkers of Sessile Serrated Adenoma/Polyps. Clin Transl Gastroenterol 2019;10:e00104.

36. Kanth P, Bronner MP, Boucher KM, et al. Gene Signature in Sessile Serrated Polyps Identifies Colon Cancer Subtype. Cancer Prev Res (Phila) 2016;9:456-65.

37. Ashktorab H, Delker D, Kanth P, et al. Molecular Characterization of Sessile Serrated Adenoma/Polyps From a Large African American Cohort. Gastroenterology 2019;157:572-574.

38. Tebbutt NC, Wilson K, Gebski VJ, et al. Capecitabine, bevacizumab, and mitomycin in first-line treatment of metastatic colorectal cancer: results of the Australasian Gastrointestinal Trials Group Randomized Phase III MAX Study. J Clin Oncol 2010;28:3191-8.

39. Xu XM, Carlson BA, Irons R, et al. Selenophosphate synthetase 2 is essential for selenoprotein biosynthesis. Biochem J 2007;404:115-20.

40. Xu XM, Yoo MH, Carlson BA, et al. Simultaneous knockdown of the expression of two genes using multiple shRNAs and subsequent knock-in of their expression. Nat Protoc 2009;4:1338-48.

41. Baum B, Georgiou M. Dynamics of adherens junctions in epithelial establishment, maintenance, and remodeling. J Cell Biol 2011;192:907-17.

42. Krendel M, Gloushankova NA, Bonder EM, et al. Myosin-dependent contractile activity of the actin cytoskeleton modulates the spatial organization of cell-cell contacts in cultured epitheliocytes. Proc Natl Acad Sci U S A 1999;96:9666-70.

43. Rustom A, Saffrich R, Markovic I, et al. Nanotubular highways for intercellular organelle transport. Science 2004;303:1007-10.

44. Osswald M, Jung E, Sahm F, et al. Brain tumour cells interconnect to a functional and resistant network. Nature 2015;528:93-8.

45. Hoffman BD, Yap AS. Towards a Dynamic Understanding of Cadherin-Based Mechanobiology. Trends Cell Biol 2015;25:803-814.

46. Michael M, Yap AS. The regulation and functional impact of actin assembly at cadherin cell-cell adhesions. Semin Cell Dev Biol 2013;24:298-307.

47. Schnittler H, Taha M, Schnittler MO, et al. Actin filament dynamics and endothelial cell junctions: the Ying and Yang between stabilization and motion. Cell Tissue Res 2014;355:529-43.

48. Yonemura S. Cadherin-actin interactions at adherens junctions. Curr Opin Cell Biol 2011;23:515-22.

49. Ayollo DV, Zhitnyak IY, Vasiliev JM, et al. Rearrangements of the actin cytoskeleton and E-cadherin-based adherens junctions caused by neoplasic transformation change cell-cell interactions. PLoS One 2009;4:e8027.

50. Gloushankova NA, Rubtsova SN, Zhitnyak IY. Cadherin-mediated cell-cell interactions in normal and cancer cells. Tissue Barriers 2017;5:e1356900.

51. Winkelman JD, Suarez C, Hocky GM, et al. Fascin- and alpha-Actinin-Bundled Networks Contain Intrinsic Structural Features that Drive Protein Sorting. Curr Biol 2016;26:2697-2706.

52. Le S, Hu X, Yao M, et al. Mechanotransmission and Mechanosensing of Human alpha-Actinin 1. Cell Rep 2017;21:2714-2723.

53. Taguchi K, Ishiuchi T, Takeichi M. Mechanosensitive EPLIN-dependent remodeling of adherens junctions regulates epithelial reshaping. J Cell Biol 2011;194:643-56.

54. Desai R, Sarpal R, Ishiyama N, et al. Monomeric alpha-catenin links cadherin to the actin cytoskeleton. Nat Cell Biol 2013;15:261-73.

55. Yao M, Qiu W, Liu R, et al. Force-dependent conformational switch of alpha-catenin controls vinculin binding. Nat Commun 2014;5:4525.

56. Seddiki R, Narayana G, Strale PO, et al. Force-dependent binding of vinculin to alpha-catenin regulates cell-cell contact stability and collective cell behavior. Mol Biol Cell 2018;29:380-388.

57. Fernandez-Sanchez ME, Barbier S, Whitehead J, et al. Mechanical induction of the tumorigenic beta-catenin pathway by tumour growth pressure. Nature 2015;523:92-5.

58. Yonemura S, Wada Y, Watanabe T, et al. alpha-Catenin as a tension transducer that induces adherens junction development. Nat Cell Biol 2010;12:533-42.

59. Przybyla L, Lakins JN, Weaver VM. Tissue Mechanics Orchestrate Wnt-Dependent Human Embryonic Stem Cell Differentiation. Cell Stem Cell 2016;19:462-475.

60. le Duc Q, Shi Q, Blonk I, et al. Vinculin potentiates E-cadherin mechanosensing and is recruited to actin-anchored sites within adherens junctions in a myosin II-dependent manner. J Cell Biol 2010;189:1107-15.

61. Whitehead J, Vignjevic D, Futterer C, et al. Mechanical factors activate beta-catenin-dependent oncogene expression in APC mouse colon. HFSP J 2008;2:286-94.

62. Stefanius K, Ylitalo L, Tuomisto A, et al. Frequent mutations of KRAS in addition to BRAF in colorectal serrated adenocarcinoma. Histopathology 2011;58:679-92.

63. Li J, Zhang S, Pei M, et al. FSCN1 Promotes Epithelial-Mesenchymal Transition Through Increasing Snail1 in Ovarian Cancer Cells. Cell Physiol Biochem 2018;49:1766-1777.

64. Jolly MK, Tripathi SC, Jia D, et al. Stability of the hybrid epithelial/mesenchymal phenotype. Oncotarget 2016;7:27067-84.

65. George SP, Chen H, Conrad JC, et al. Regulation of directional cell migration by membrane-induced actin bundling. J Cell Sci 2013;126:312-26.

66. Ubelmann F, Chamaillard M, El-Marjou F, et al. Enterocyte loss of polarity and gut wound healing rely upon the F-actin-severing function of villin. Proc Natl Acad Sci U S A 2013;110:E1380-9.

67. Dhomen N, Reis-Filho JS, da Rocha Dias S, et al. Oncogenic Braf induces melanocyte senescence and melanoma in mice. Cancer Cell 2009;15:294-303.

68. Zou M, BinEssa HA, Al-Malki YH, et al. beta-Catenin Attenuation Inhibits Tumor Growth and Promotes Differentiation in a BRAF(V600E)-Driven Thyroid Cancer Animal Model. Mol Cancer Ther 2021;20:1603-1613.

69. Cho SW, Kim YA, Sun HJ, et al. Therapeutic potential of Dickkopf-1 in wild-type BRAF papillary thyroid cancer via regulation of beta-catenin/E-cadherin signaling. J Clin Endocrinol Metab 2014;99:E1641-9.

70. Murakami T, Mitomi H, Saito T, et al. Distinct WNT/beta-catenin signaling activation in the serrated neoplasia pathway and the adenoma-carcinoma sequence of the colorectum. Mod Pathol 2015;28:146-58.

71. Yozu M, Kem M, Cenaj O, et al. Loss of expression of MLH1 in non-dysplastic crypts is a harbinger of neoplastic progression in sessile serrated adenomas/polyps. Histopathology 2019;75:376-384.

72. Fennell L, Dumenil T, Wockner L, et al. Integrative Genome-Scale DNA Methylation Analysis of a Large and Unselected Cohort Reveals 5 Distinct Subtypes of Colorectal Adenocarcinomas. Cell Mol Gastroenterol Hepatol 2019;8:269-290.

73. Schoumacher M, El-Marjou F, Lae M, et al. Conditional expression of fascin increases tumor progression in a mouse model of intestinal cancer. Eur J Cell Biol 2014;93:388-95.

74. Kriegl L, Vieth M, Kirchner T, et al. Up-regulation of c-MYC and SIRT1 expression correlates with malignant transformation in the serrated route to colorectal cancer. Oncotarget 2012;3:1182-93.

75. Zhuang D, Mannava S, Grachtchouk V, et al. C-MYC overexpression is required for continuous suppression of oncogene-induced senescence in melanoma cells. Oncogene 2008;27:6623-34.

76. Feng L, Li J, Bu X, et al. BRAF(V600E) dictates cell survival via c-Myc-dependent induction of Skp2 in human melanoma. Biochem Biophys Res Commun 2020;524:28-35.

77. Tabor V, Bocci M, Alikhani N, et al. MYC synergizes with activated BRAFV600E in mouse lung tumor development by suppressing senescence. Cancer Res 2014;74:4222-9.

78. Freedman SL, Suarez C, Winkelman JD, et al. Mechanical and kinetic factors drive sorting of F-actin cross-linkers on bundles. Proc Natl Acad Sci U S A 2019;116:16192-16197.

79. Benham-Pyle BW, Pruitt BL, Nelson WJ. Cell adhesion. Mechanical strain induces E-cadherin-dependent Yap1 and beta-catenin activation to drive cell cycle entry. Science 2015;348:1024-7.

80. Roper JC, Mitrossilis D, Stirnemann G, et al. The major beta-catenin/E-cadherin junctional binding site is a primary molecular mechano-transductor of differentiation in vivo. Elife 2018;7:e33381.

81. Li JXH, Tang VW, Brieher WM. Actin protrusions push at apical junctions to maintain E-cadherin adhesion. Proc Natl Acad Sci U S A 2020;117:432-438.

82. Naphade S, Sharma J, Gaide Chevronnay HP, et al. Brief reports: Lysosomal cross-correction by hematopoietic stem cell-derived macrophages via tunneling nanotubes. Stem Cells 2015;33:301-9.

83. Jia D, Jolly MK, Tripathi SC, et al. Distinguishing mechanisms underlying EMT tristability. Cancer Converg 2017;1:2.

84. Niewiadomska P, Godt D, Tepass U. DE-Cadherin is required for intercellular motility during Drosophila oogenesis. J Cell Biol 1999;144:533-47.

85. Poznansky MC, Olszak IT, Foxall R, et al. Active movement of T cells away from a chemokine. Nat Med 2000;6:543-8.

86. Vianello F, Olszak IT, Poznansky MC. Fugetaxis: active movement of leukocytes away from a chemokinetic agent. J Mol Med (Berl) 2005;83:752-63.

87. Dent EW, Gupton SL, Gertler FB. The growth cone cytoskeleton in axon outgrowth and guidance. Cold Spring Harb Perspect Biol 2011;3.

88. Mathew S, George SP, Wang Y, et al. Potential molecular mechanism for c-Src kinase-mediated regulation of intestinal cell migration. J Biol Chem 2008;283:22709-22.

89. Patnaik S, George SP, Pham E, et al. By moonlighting in the nucleus, villin regulates epithelial plasticity. Mol Biol Cell 2016;27:535-48.

90. Humtsoe JO, Koya E, Pham E, et al. Transcriptional profiling identifies upregulated genes following induction of epithelial-mesenchymal transition in squamous carcinoma cells. Exp Cell Res 2012;318:379-90.

91. Wang Y, George SP, Roy S, et al. Both the anti- and pro-apoptotic functions of villin regulate cell turnover and intestinal homeostasis. Sci Rep 2016;6:35491.

92. Bado I, Nikolos F, Rajapaksa G, et al. ERbeta decreases the invasiveness of triple-negative breast cancer cells by regulating mutant p53 oncogenic function. Oncotarget 2016;7:13599-611.

93. Hugh TJ, Dillon SA, Taylor BA, et al. Cadherin-catenin expression in primary colorectal cancer: a survival analysis. Br J Cancer 1999;80:1046-51.

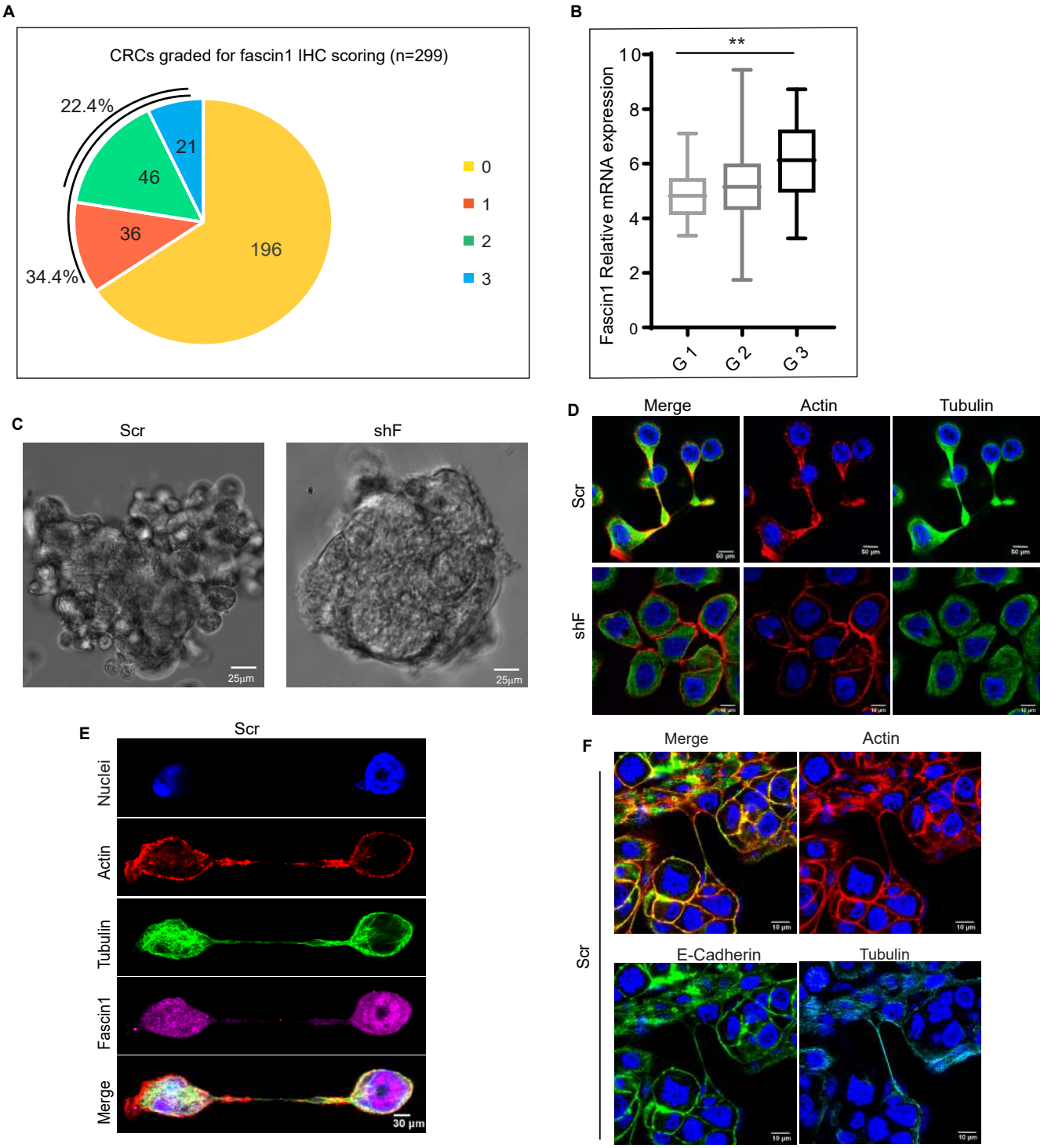
A
CRCs graded for fascin1 IHC scoring (n=299)
22.4%
34.4%
21
46
36
196
0
1
2
3
B
**
Fascin1 Relative mRNA expression
10
8
6
4
2
0
G1
G2
G3
C
Scr
shF
25µm
25µm
D
Merge
Actin
Tubulin
Scr
shF
E
Scr
Nuclei
Actin
Tubulin
Fascin1
Merge
30 µm
F
Merge
Actin
Scr
E-Cadherin
Tubulin

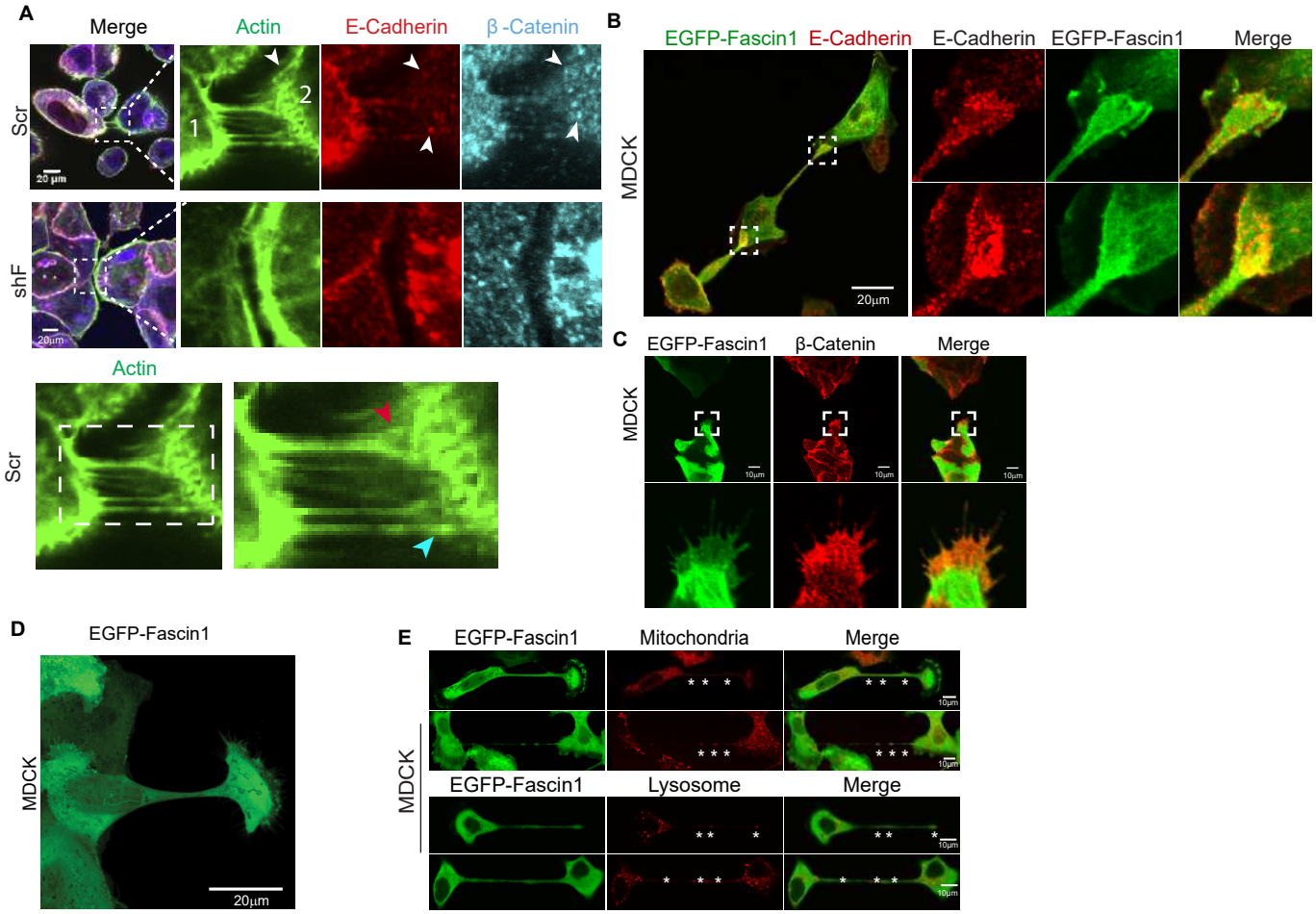
A
Merge
Actin
E-Cadherin
β -Catenin
Scr
shF
1
2
20 µm
Actin
Scr
B
EGFP-Fascin1
E-Cadherin
E-Cadherin
EGFP-Fascin1
Merge
MDCK
20µm
C
EGFP-Fascin1
β-Catenin
Merge
MDCK
10µm
D
EGFP-Fascin1
MDCK
20µm
E
EGFP-Fascin1
Mitochondria
Merge
MDCK
EGFP-Fascin1
Lysosome
Merge
10µm

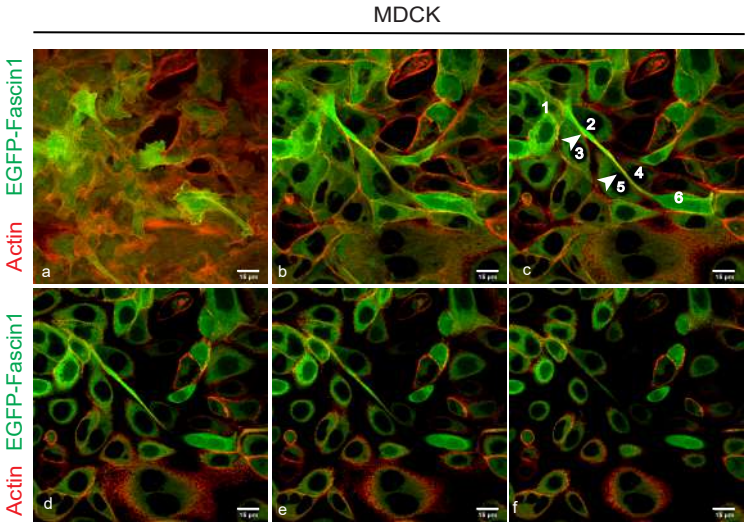
MDCK
EGFP-Fascin1
Actin
EGFP-Fascin1
Actin
a
b
c
d
e
f
1
2
3
4
5
6

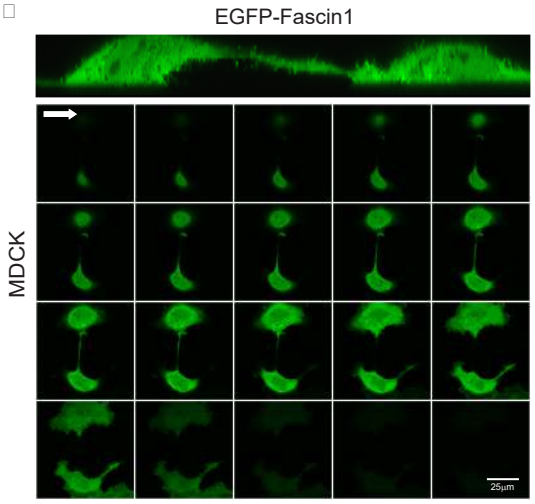
EGFP-Fascin1
MDCK
25μm

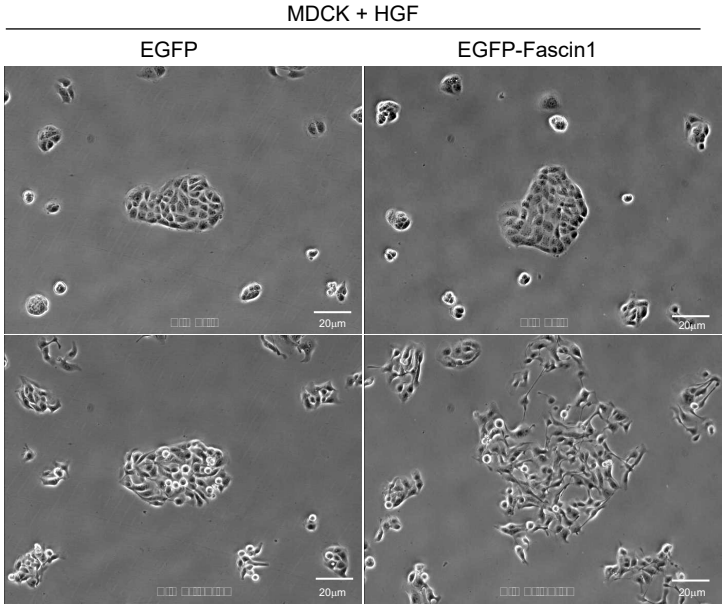
MDCK + HGF
EGFP
EGFP-Fascin1
20μm
20μm
20μm
20μm

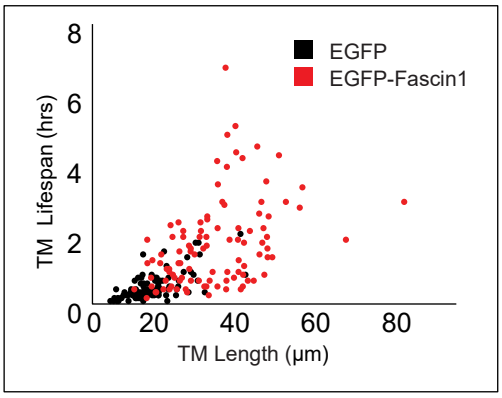
EGFP
EGFP-Fascin1
TM Lifespan (hrs)
TM Length (μm)
0
2
4
6
8
0
20
40
60
80

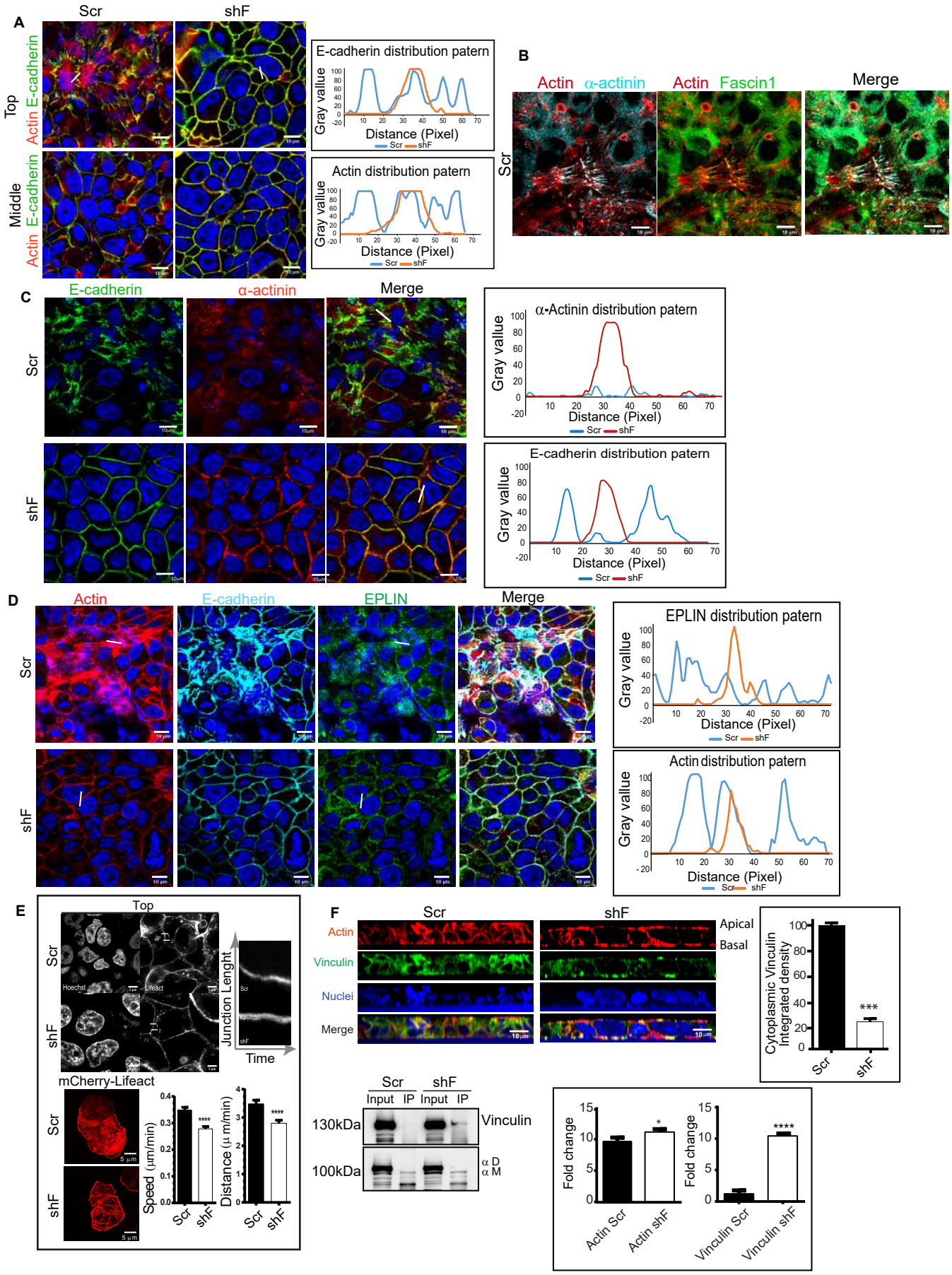
A
Scr
shF
Top
E-cadherin
Actin
Middle
E-cadherin
Actin
E-cadherin distribution patern
Actin distribution patern
Gray value
Distance (Pixel)
Scr
shF
B
Actin
α-actinin
Actin
Fascin1
Merge
Scr
C
E-cadherin
α-actinin
Merge
Scr
shF
α-Actinin distribution patern
E-cadherin distribution patern
D
Actin
E-cadherin
EPLIN
Merge
Scr
shF
EPLIN distribution patern
Actin distribution patern
E
Top
Scr
shF
Hoechst
Lifeact
Junction Lenght
Time
mCherry-Lifeact
Speed (µm/min)
Distance (µ m/min)
F
Scr
shF
Actin
Vinculin
Nuclei
Merge
Apical
Basal
Cytoplasmic Vinculin Integrated density
Input
IP
130kDa
100kDa
Vinculin
α D
α M
Fold change
Actin Scr
Actin shF
Vinculin Scr
Vinculin shF

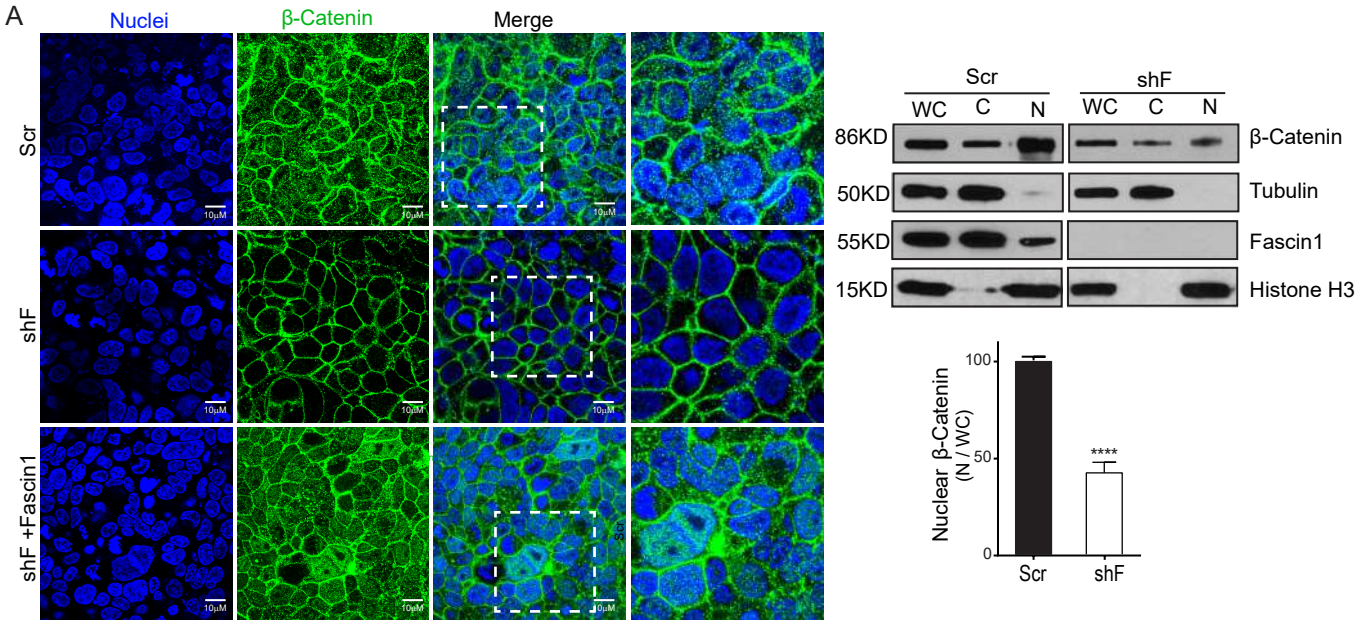
A
Nuclei
β-Catenin
Merge
Scr
shF
shF +Fascin1
10μM
Scr
shF
WC
C
N
86KD
50KD
55KD
15KD
β-Catenin
Tubulin
Fascin1
Histone H3
Nuclear β-Catenin (N / WC)
100
50
0
****
Scr
shF

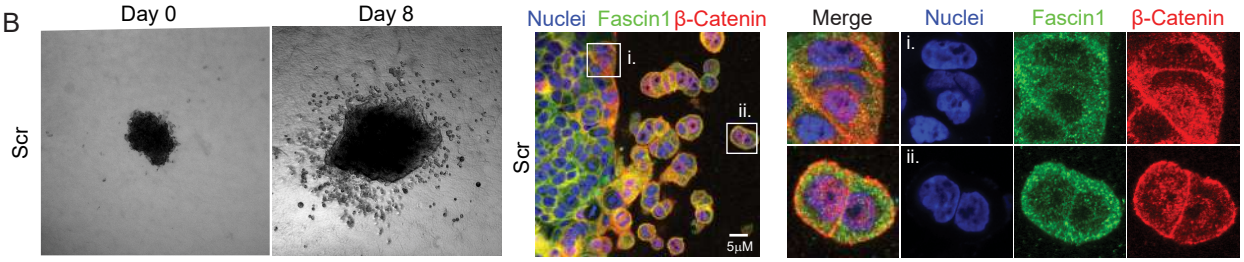
B
Day 0
Day 8
Scr
Nuclei
Fascin1
β-Catenin
Merge
i.
ii.
5μM

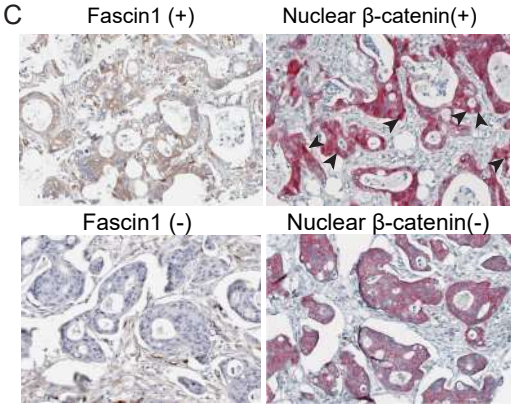
C
Fascin1 (+)
Nuclear β-catenin(+)
Fascin1 (-)
Nuclear β-catenin(-)

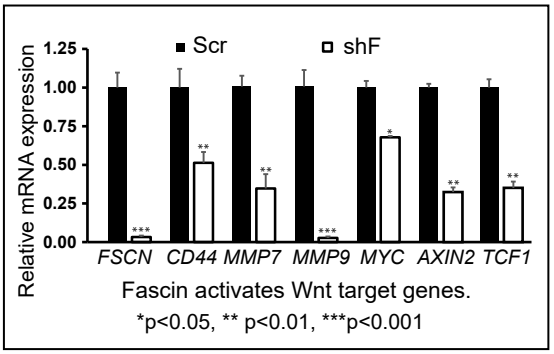
D
Scr
shF
Relative mRNA expression
1.25
1.00
0.75
0.50
0.25
0.00
FSCN
CD44
MMP7
MMP9
MYC
AXIN2
TCF1
Fascin activates Wnt target genes.
*p<0.05, ** p<0.01, ***p<0.001

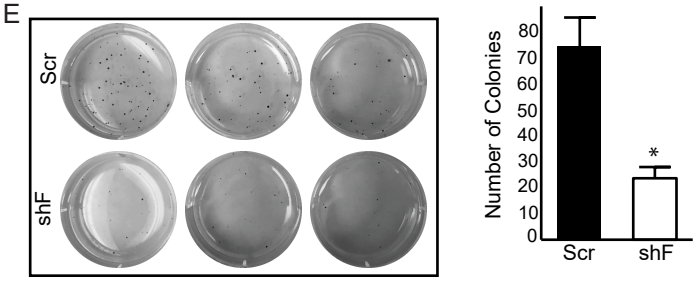
E
Scr
shF
Number of Colonies
80
70
60
50
40
30
20
10
0
*
Scr
shF

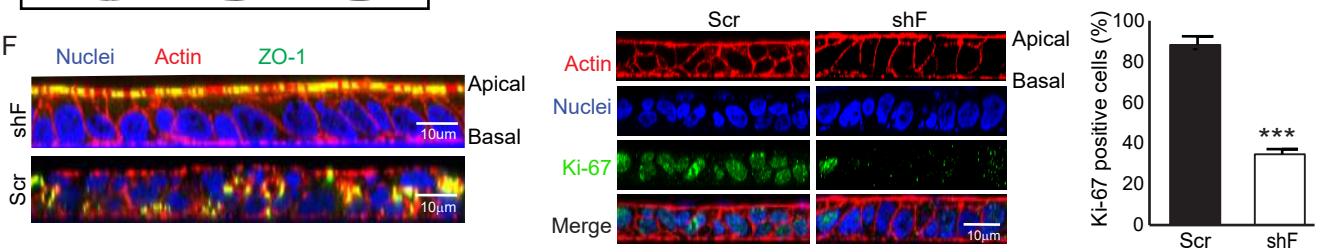
F
Nuclei
Actin
ZO-1
shF
Scr
Apical
Basal
10um
10μm
Actin
Nuclei
Ki-67
Merge
Ki-67 positive cells (%)
100
80
60
40
20
0
***
Scr
shF

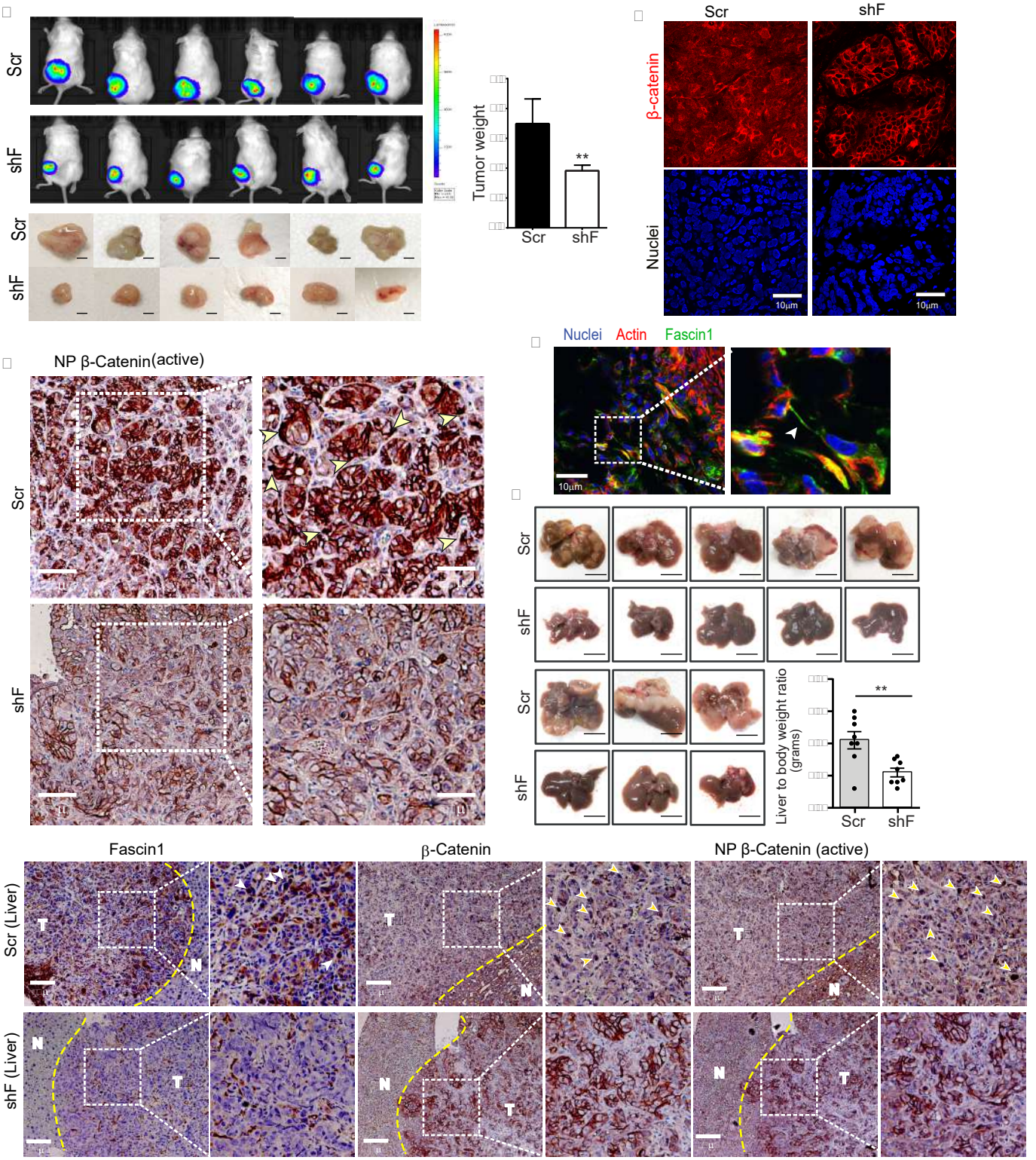
Scr
shF
Tumor weight
**
Scr
shF
β-catenin
Nuclei
10μm
NP β-Catenin(active)
Nuclei Actin Fascin1
Liver to body weight ratio (grams)
Fascin1
β-Catenin
NP β-Catenin (active)
Scr (Liver)
shF (Liver)
T
N

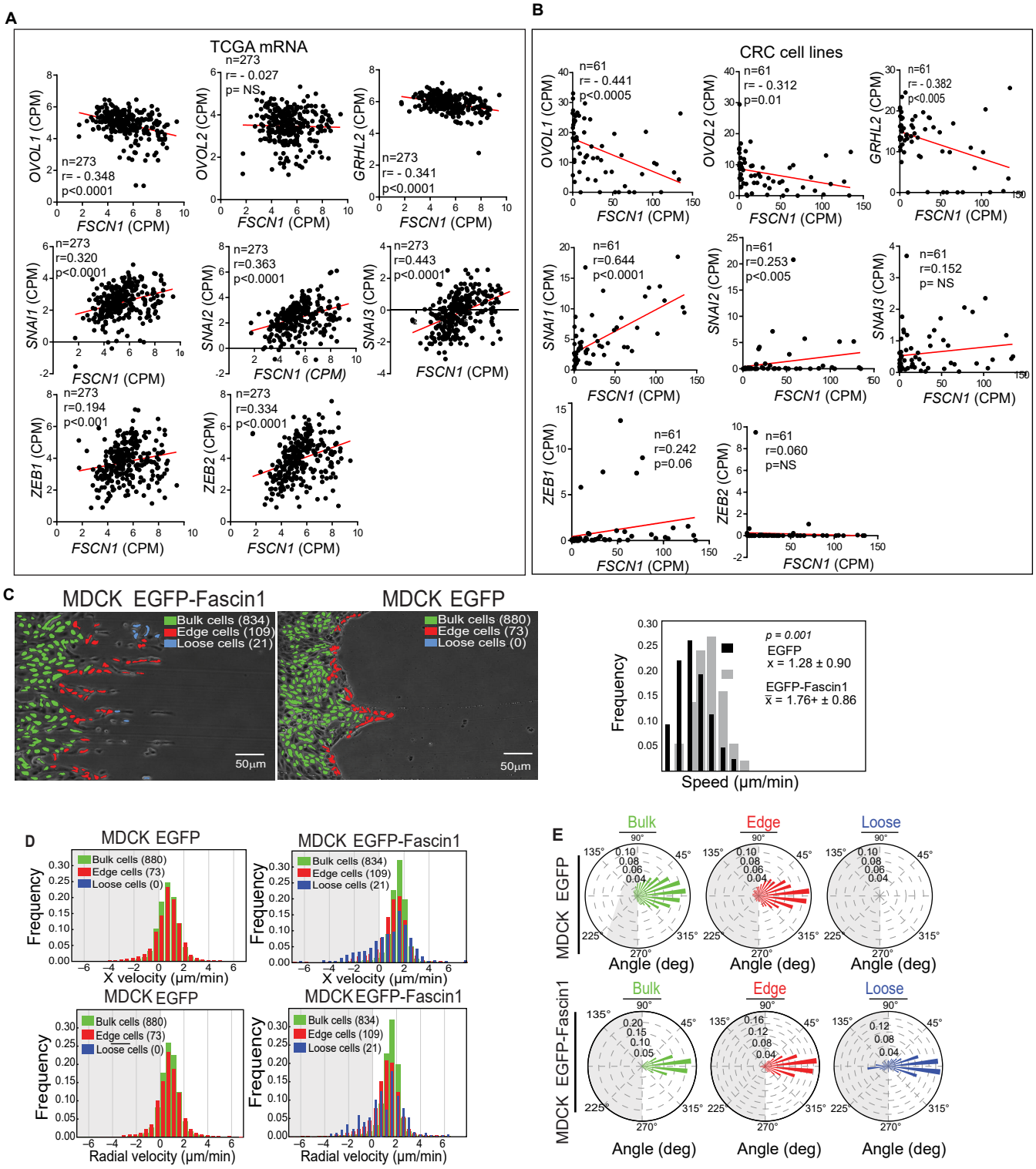
A
TCGA mRNA
n=273
r= - 0.027
p= NS
n=273
r= - 0.348
p<0.0001
n=273
r= - 0.341
p<0.0001
n=273
r=0.320
p<0.0001
n=273
r=0.363
p<0.0001
n=273
r=0.443
p<0.0001
n=273
r=0.194
p<0.001
n=273
r=0.334
p<0.0001
OVOL1 (CPM)
OVOL2 (CPM)
GRHL2 (CPM)
SNAI1 (CPM)
SNAI2 (CPM)
SNAI3 (CPM)
ZEB1 (CPM)
ZEB2 (CPM)
FSCN1 (CPM)
B
CRC cell lines
n=61
r= - 0.441
p<0.0005
n=61
r= - 0.312
p=0.01
n=61
r= - 0.382
p<0.005
n=61
r=0.644
p<0.0001
n=61
r=0.253
p<0.005
n=61
r=0.152
p= NS
n=61
r=0.242
p=0.06
n=61
r=0.060
p=NS
C
MDCK EGFP-Fascin1
Bulk cells (834)
Edge cells (109)
Loose cells (21)
50µm
MDCK EGFP
Bulk cells (880)
Edge cells (73)
Loose cells (0)
50µm
p = 0.001
EGFP
x = 1.28 ± 0.90
EGFP-Fascin1
x̄ = 1.76+ ± 0.86
Frequency
Speed (µm/min)
D
MDCK EGFP
MDCK EGFP-Fascin1
Bulk cells (880)
Edge cells (73)
Loose cells (0)
Bulk cells (834)
Edge cells (109)
Loose cells (21)
Frequency
X velocity (µm/min)
Radial velocity (µm/min)
E
Bulk
Edge
Loose
MDCK EGFP
MDCK EGFP-Fascin1
Angle (deg)